Mechanisms underlying the abnormal respiratory-sympathetic phenotype of the Spontaneously Hypertensive Rat

Tonique Newbold (BSc.)

Macquarie Medical School

Faculty of Medicine, Health, and Human Sciences

Macquarie University

NSW Australia

Presented for the degree of Master of Research under the supervision of Simon McMullan, Peter Burke, and Cara Hildreth.

February 2022

Declaration

The work presented in this thesis was undertaken in the Faculty of Medicine, Health, and Human Sciences at Macquarie University, Sydney, Australia. The material in this thesis is my own original work, except where referenced in the text, and has not been previously submitted for any other degree or diploma in any university. To the best of my knowledge and belief, the thesis contains no material previously published or written by another person except where due reference is made in the thesis itself.

Experimental procedures were carried out by myself, with assistance from others as detailed in acknowledgements section. Ethics approval was obtained for all animal experiments (Macquarie Animal Ethics Committee Authority 2018-024), and work was conducted in accordance with the Australian Code of Practice for the Care and Use of Animals for Scientific Purposes (2013), the NSW Animal Research Act (1985), and the NSW Animal Research Regulation (2021).

11 February 2022

Acknowledgements

This project was funded by Macquarie University, including a scholarship for living allowances during my candidature. I am incredibly grateful for the opportunities I have been offered and have had a fantastic experience studying here. I am extremely proud to be part of the MQ community!

To my amazing supervisor, Simon McMullan. You are the best teacher I have ever had. Thank you for your endless advice, support, and encouragement throughout this project. It has been such a challenging year, there is no way I could have made it through without you.

This project would not have been possible without the surgical expertise of Anita Turner. I had a great time working with you and learned so many interesting things. Thank you for going above and beyond to make sure all my experiments were completed.

Harry Carey and Greg Smith provided technical support with Spike video capture. It seemed like such a simple idea but ended up being a much more complicated process than I (or anyone else) anticipated! Thanks for all your help.

Research assistant Andrea Kuriakose assisted with histology, imaging, and animal care. You are so efficient and organised, and always looking for ways to help. This massively reduced my workload (and stress!) throughout this project. Thank you for everything.

I'd also like to thank my co-supervisors, Peter Burke and Cara Hildreth, and fellow HDR students Christine Saleeba, April Gregson, and Stephanie Kennett, for their moral and emotional support this year. I am so fortunate to be surrounded by such wonderful people.

Finally, my parents Ian Newbold and Karen Paull, who always encouraged me to pursue my dreams. So many people told me this was impossible, but you never doubted me. You always knew I was capable of anything I set my mind to. Thank you for always believing in me.

Table of Contents

Abstract

There is an established link between sympathetic dysregulation and hypertension, with animal models showing a temporal phase shift in peak sympathetic activity from the post-inspiratory (post-I) period to late inspiration. The mechanism driving altered respiratory-sympathetic coupling in spontaneously hypertensive rats (SHR) is still unknown. It has been suggested that pathways driving post-I activity are overactive in SHRs, resulting in premature sympathetic activation. Alternatively, it has been suggested that abnormal excitatory connections between inspiratory neurons in PreBötC and the RVLM cause an increase in sympathetic activity during inspiration.

This project used electrophysiological nerve recordings to compare vagal and sympathetic nerve activity between SHR and WKY rats. Additionally, larynx muscle movement was recorded using videography to directly measure post-I laryngeal adduction. It was expected that peak vagus activity would also be phase-shifted in SHRs, but results show similar timing of laryngeal adduction and vagal post-I activity in both strains, despite peak sympathetic activity occurring earlier in SHRs. It was also found that WKYs have a temporal phase shift in vagal post-I activity during hypoxemia, while SHRs showed no change. Hypoxemia delays sympathetic activity in SHRs, while the effect in WKYs is variable and shows no consistent pattern.

These findings indicate thar sympathetic and vagal post-I activity are separate mechanisms that can be altered independently in response to homeostatic challenge. As vagal post-I activity is not phase shifted in SHRs, this supports the hypothesis that their altered respiratory-sympathetic coupling is due to a mechanism acting on the sympathetic nervous system directly, not one affecting post-I activity in general.

List of Figures

List of Abbreviations

AP: Arterial Pressure
BötC: Bötzinger complex
CNVII: cranial nerve 7 (facial)
CNX: cranial neve 10 (vagus)
CPG: central pattern generator
cVRG: caudal ventral respiratory group
DLC: Deep Lab Cut
EMG: electromyography
i.m. intramuscular
i.v.: intravenous
IRt/PiCo: intermediate reticular nucleus/post-inspiratory complex
KF: Kölliker-Fuse nucleus
LC: laryngeal constrictors
NA: nucleus ambiguus
NTS: nuclei of solitary tract
PBS: phosphate-buffered saline
PCA: posterior cricoarytenoid muscles
PFA: paraformaldehyde
PNA: phrenic nerve activity
Post-I: post-Inspiration
preBötC: pre-Bötzinger complex
PRG: pontine respiratory group
RLN: recurrent laryngeal nerve
RTN/pFRG: retrotrapezoid nucleus/parafacial respiratory group
RVLM: rostral ventrolateral medulla
rVRG: rostral ventral respiratory group
s.c. subcutaneous
SHR: spontaneously hypertensive rat
SNA: sympathetic nerve activity
SNS: sympathetic nervous system
TE: expiration time
TI: inspiration time
Ttot: total respiratory cycle length (TI+TE)
VNA: vagus nerve activity
VRC: ventral respiratory column
WKY: Wistar-Kyoto rat

1. Introduction

1.1 Overview

Respiration is a complex process involving many brain regions, nerve pathways, and muscle groups. As it is essential for survival, respiratory activity must be coordinated with other bodily functions. Cardiovascular activity is one example: heart rate and blood pressure fluctuations occur in synchronicity with the respiratory cycle [1].

The sympathetic nervous system is involved in coordination between respiration and blood pressure. Sympathetic activity peaks immediately after inspiration (the post-inspiratory, or post-I period), in a phenomenon called respiratory-sympathetic coupling [1]. Vagus nerve activity also peaks during post-I, which is thought to drive post-inspiratory laryngeal adduction via the recurrent laryngeal nerve [5] [6]. The term 'post-I activity' has been used to describe this peak amplitude in both vagal and sympathetic nerve activities, which the assumption that both are driven by the same mechanism. Alternatively, it has been suggested that vagal and sympathetic post-I may be generated by distinct independent mechanisms [2]. To avoid confusion, the terms 'vagal post-I activity' and 'respiratory-sympathetic coupling' will be used to describe the peak in vagal and sympathetic activity often seen during post-inspiration.

Hypertension has been associated with increased sympathetic activity, both in clinical studies [3] [4] [5] and rodent models of hypertension [6] [7] [8]. In the spontaneous hypertensive rat (SHR), there is a respiratory phase shift in respiratory-sympathetic coupling, with peak sympathetic activity occurring earlier than normotensive rats, during late inspiration rather than the post-I period [6]. This occurs prior to development of hypertension, as shown in sympathetic recordings of juvenile pre-hypertensive SHRs [7]. Inhibition of C1 cardiovascular neurons in the rostral ventrolateral medulla (RVLM) in SHRs reduces the amplitude of respiratory-sympathetic coupling, shifts time of peak sympathetic activity back into the post-I period, and reduces arterial blood pressure [8]. This is evidence of a causal relationship between amplified-respiratory sympathetic coupling and hypertension.

The source of post-I vagal activity is still under investigation. Inhibitory inputs from the Bötzinger complex (BötC) and pre-Bötzinger complex (preBötC) suppress laryngeal motor neuron activity during inspiration and late expiration [9]. In this model excitatory inputs play a minimal role in respiratory laryngeal adduction, and vagal post-I activity is due to cessation of inhibition at the end of inspiration, in a post-inhibitory rebound mechanism [2]. More recently, neurons in the intermediate-reticular nucleus (IRt) have been suggested as a possible source of excitatory post-I drive to vagal motoneurons, as inhibition of this region abolishes vagal [10] and sympathetic post-I activity [11]. It is thus suggested that neurons in the IRt play a role in the coordination of vagal and sympathetic activity with the respiratory cycle.

While amplified respiratory-sympathetic coupling in SHRs has been well established, the neural mechanisms underlying this dysfunction have not been defined. One possibility is that reconfiguration of the pathways that underlie post-I activity cause sympathetic activity to peak earlier in the respiratory cycle (post-I neurons in the Kölliker-Fuse nucleus (KF) or IRt, discussed below, are plausible candidates), as inhibition of either region causes a reduction in post-I activity [11] [12]. Alternatively, it has been proposed that plastic enhancement of excitatory connections between preBötC and the RVLM exist in SHRs [13]. If this were the case, activity in the preBötC would cause a peak in sympathetic activity during inspiration.

A brief review of the generally accepted model of central respiratory and sympathetic control follows.

1.2 Respiration

'Normal' breathing (eupnoea) consists of three distinct phases- inspiration, post-inspiration, and expiration [12]. The main purpose of respiration is to regulate oxygen and carbon dioxide levels. This is extremely important as the body has only a limited capacity to store oxygen, and brain damage can occur after just minutes of oxygen deprivation [14]. Respiratory failure is a common cause of death in neurodegenerative diseases, and dysfunction of neural control is present in many respiratory disorders such as sleep apnoea and SIDs [15].

1.2.1 Diaphragm

The diaphragm is the main muscle that drives inspiration in mammals. It spans the base of the ribcage, separating the thoracic and abdominal cavities. Diaphragm activation during inspiration expands the space inside the chest, creating negative pressure and drawing air into the lungs [16]. Electromyography (EMG) can be used to measure diaphragm muscle activity: periods of EMG activity and silence give a clear indicator of inspiration and expiration respectively. The motor neurons driving diaphragm activity have cell bodies located in lamina IX of the spinal cord at cervical vertebrae 3-5, with axons travelling along the phrenic nerve [16]. The phrenic nerve also displays a distinct pattern of bursting and silencing activity similar to diaphragm EMG.

1.2.2 Larynx

The larynx is comprised of several different muscles, as depicted in Figure 1.1 below. During inspiration, the posterior cricoarytenoid muscles (PCA) contract, causing the thyroarytenoids (also known as the vocal cords) to separate, opening the throat and allowing air to pass through [2]. Immediately after this, during the post-I period, a group of muscles called the laryngeal constrictors (LC) contract. LCs include the thyroarytenoids, the lateral cricoarytenoids, and the interarytenoids. This causes partial adduction of the larynx, increasing air pressure inside the lungs allowing for more efficient gas exchange. Then, during expiration, the diaphragm and larynx relax allowing for air to be expelled [16].

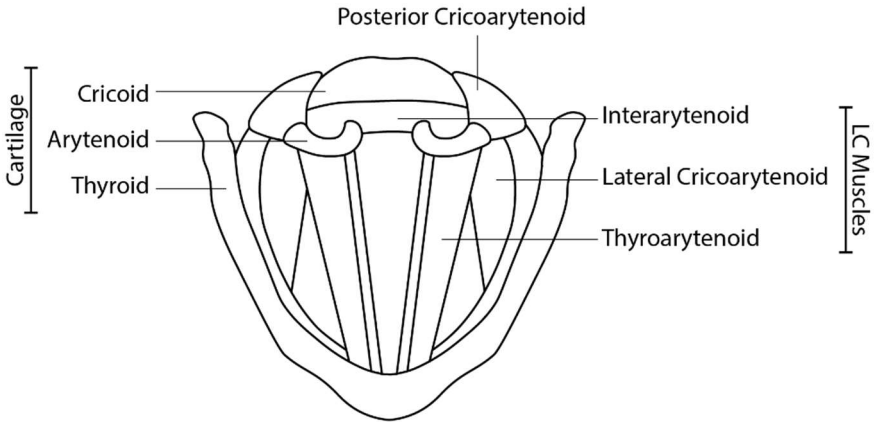

Figure 1.1: Muscles and cartilage of the larynx. LC=laryngeal constrictor muscles

Laryngeal motor neuron cell bodies are located in the medullary nucleus ambiguus (NA) [2], with axons running along the recurrent laryngeal (RLN) branch of the vagus nerve (cranial nerve X) [17]. During the post-I period, a spike of activity is seen in the RLN which is thought to drive LC muscle activity and laryngeal adduction [11] [2].

1.2.3 Other Respiratory Muscles

Many other muscles of the mouth, tongue, and throat are also involved in respiration. Cranial nerve VII (facial nerve) provides motor and sensory inputs to the muscles of the face, inside of the mouth, and anterior tongue [18]. Cranial nerve XII (hypoglossal nerve) provides motor input to the tongue [19]. Cranial nerve X (vagus nerve) has several branches, innervating the larynx as described above, but also provides motor input to the pharynx via the pharyngeal branch [17]. These are outside the scope of this project, which focuses on the diaphragm and larynx only.

1.3 Respiratory Control

1.3.1 Central Pattern Generator

Respiration is driven by a series of inhibitory and excitatory interneurons that generate a pattern of rhythmic activity [20]. This central pattern generator (CPG) is located in the bilateral ventral respiratory column (VRC) of the medulla, with several interconnections with the pontine respiratory group (PRG) via the nucleus of the solitary tract (NTS). CPG activity in the VRC drives activity in cranial and spinal motor neurons, which innervate the larynx and diaphragm respectively. Many regions outside of the brainstem also influence CPG activity, including the cerebellum, hypothalamus, and the sensorimotor cortex [20]. This ensures homeostasis by altering respiration in response to an organism's constantly changing needs. Some of these pathways are illustrated in Figure 1.2 and described in further detail below.

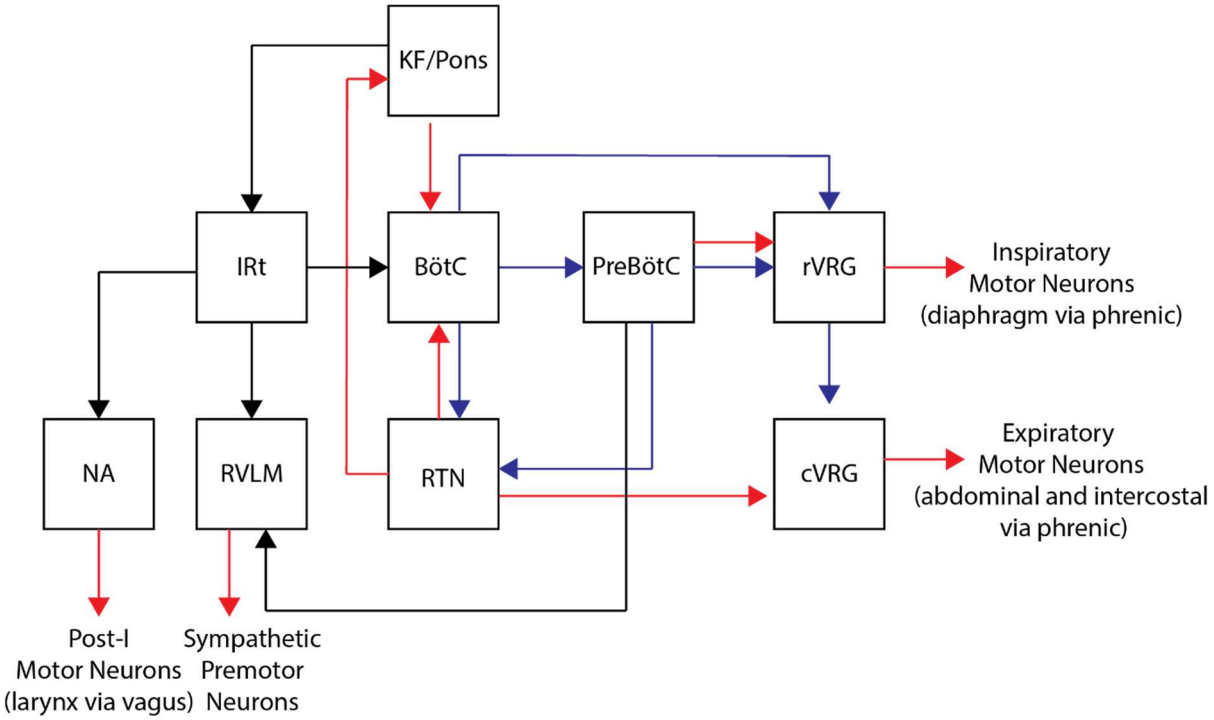

Figure 1.2: Major pathways that drive respiratory activity. Red arrows=excitatory inputs, blue arrows=inhibitory inputs, black arrows=proposed inputs. IRt=intermediate reticular nucleus, RVLM= rostral ventrolateral medulla NA=nucleus ambiguus, KF=Kölliker-Fuse nucleus, BötC= Bötzinger complex, PreBötC= pre-Bötzinger complex, rVRG=rostral ventral respiratory group, cVRG=caudal ventral respiratory group, RTN=retrotrapezoid nucleus (or parafacial respiratory group) – Modified from Toor et.al. (2019) [11].

1.3.2 Pre-Bötzinger Complex

PreBötC contains a distinct subpopulation of glutamatergic bilaterally projecting neurons that display rhythmic oscillations in activity [21]. PreBötC also contains glycinergic and GABAergic neurons that inhibit activity of expiratory premotor neurons during inspiration [9] [20]. PreBötC is active during inspiration [10], and inhibition of the area results in apnoea and loss of phrenic bursting [21]. Due to this, and its capacity to generate innate bursting activity *in vitro*, PreBötC is widely considered to be the source of inspiratory rhythm [13].

1.3.3 Bötzinger Complex

BötC is located immediately rostral to PreBötC. Active during expiration, BötC inhibits the activity of inspiratory motor neurons [2] via glycinergic and GABAergic projections to PreBötC and the rostral ventral respiratory group (rVRG) [20]. BötC is considered to be the source of eupneic expiration as its activity relaxes the diaphragm [16] and PCA [2] muscles allowing air to be expelled.

1.3.4 Rostral Ventral Respiratory Group

The rVRG is immediately caudal to BötC and PreBötC, and contains bulbospinal premotor inspiratory neurons [20]. Activity in the rVRG is largely shaped by excitatory input from PreBötC during inspiration, and inhibitory input from BötC during expiration as described above. The pattern of inspiratory burst and expiratory silencing in the phrenic nerve is driven by BötC/pre BötC mediated rVRG activity [20].

1.3.5 Caudal Ventral Respiratory Group

The caudal ventral respiratory group (cVRG) contains bulbospinal premotor neurons that drive expiratory muscles [20]. During eupnoea, expiration is usually a passive function characterised by a lack of activity. However, during metabolic stress, some muscles (e.g. abdominal, intercostal) are recruited during expiration [22]. The cVRG is inhibited during inspiration by the rVRG, and expiratory activity is shaped by chemoreceptive neurons in the retrotrapezoid nucleus (RTN), as described below.

1.3.6 Retrotrapezoid Nucleus

The RTN, also referred to as the parafacial respiratory group (pFRG), contains intrinsically CO_2-sensitive neurons that alter CPG activity via excitatory glutamatergic projections to preBötC, cVRG, and pontine respiratory regions [20]. RTN is thought to trigger active respiration by increasing the activity in expiratory premotor neurons in the cVRG in response to CO_2 or pH levels [22]

1.3.7 Kölliker-Fuse Nucleus

The Kölliker-Fuse nucleus (KF), located in the pons, has several synaptic connections to the NA and rVRG [2]. The KF is essential for the generation of post-I activity, as previous studies in brainstem-spinal cord preparations have found that removal of the pons results in abolishment of post-I vagus activity, while phrenic inspiration and expiration activity persists [12]. Further experiments found that inhibition of the KF with isoguvacine had similar results, abolishing post-I activity in the RLN, and decreasing laryngeal adduction, as indicated by

subglottal pressure. They also found that excitation of the KF with glutamate increased post-I RLN activity and sustained laryngeal adduction [23].

1.3.8 Intermediate Reticular Nucleus

The medullary intermediate reticular nucleus (IRt), also called the post-inspiratory complex (PiCo), contains a population of excitatory cholinergic neurons [10] [11]. The IRt has been suggested as the potential source of vagal post-I activity, as inhibition in this region abolishes post-I activity, while excitation stimulates a spike in vagal activity regardless of respiratory phase [10]. IRt inhibition has also been shown to reduce sympathetic activity [11]. However, more recent studies have found that vagal post-I activity returns during hypoxemia despite inhibition of the IRt [11]. This indicates that the IRt in not the source of post-I activity, and may instead act as a pre-motor relay station involved in respiratory activity with other inputs, perhaps originating in KF [11]. This is supported by the fact that IRt inhibition also supressed the vagal response to fictive swallow [11].

1.4 Sympathetic Nervous System

1.4.1 Overview

The sympathetic nervous system (SNS) forms part of the autonomic nervous system responsible for regulating a range of different bodily functions to maintain homeostasis. The SNS exhibits ongoing activity that maintains tonic vasomotor tone, while its further activation prepares the body for intense physical demand by redirecting oxygen-rich blood to needed areas [24].

The SNS comprises of short, preganglionic neurons with cell bodies located in the spinal cord at T1-L2, that synapse on to neurons in chains of sympathetic ganglia that run down each side of the spine. These junctions use the neurotransmitter acetylcholine, acting on nicotinic receptors [24]. Post-synaptic sympathetic neurons have long axons, and travel to a range of different effector sites all over the body. In most cases sympathetic postganglionic neurons release norepinephrine, which acts on adrenergic receptors in target organs [25], although sweat glands and hair follicles are effected by acetylcholine [24].

Increased SNS activation maximises energy availability by inhibiting less salient functions (e.g. digestion and urination), increasing glucose and glycogen production in the liver, and reducing insulin production in the pancreas. The pupils dilate, sweat glands increase production, and hair follicles become erect. To increase oxygen availability, heart rate and contraction force increase, improving cardiac output, and vascular smooth muscle contracts, collectively increasing blood pressure. The lungs are also affected by SNS activation, stimulating bronchodilation to increase airflow [24].

1.4.2 Sympathetic dysregulation in human hypertension

The sympathetic nervous system is overactive in people with hypertension [26], especially younger patients [5]. In other cardiac conditions, increased sympathetic activity (measured by cardiac norepinephrine output) is associated with lower survival rates [27].

However, these changes to sympathetic activity are not uniform. In hypertensive patients, increased activity is seen in the postganglionic sympathetic nerve fibres that innervate blood vessels in skeletal muscle [3] but not in those that innervate the skin [28]. Conversely, stress-related sympathetic activation shows an increase in skin activation but no change to skeletal muscle [5]. This indicates that the sympathetic nervous system is selective, with changes localised to selected organs and systems. For example, hypertensive patients have increased norepinephrine in the heart and kidneys [4].

1.4.3 Sympathetic dysregulation in animal models of hypertension

There are many existing animal models of hypertension. Hypertension can be induced by surgically clamping renal arteries [29] [30], placing animals in a stressful environment [31], or high-salt diet [32]. Pharmacological hypertension can be induced by administering drugs such as nitric oxide synthase inhibitors and angiotensin II [33]. Transgenic models are also available, such as overexpression of the mouse *Ren-2* gene in rats [34]. The most commonly used animal model of hypertension is the spontaneously hypertensive rat (SHR) [35].

SHRs have been selectively bred for hypertension [36], and show many similarities to essential hypertension in humans, including increased sympathetic activity [37]. Sympathetic activity not only increased in amplitude, but also showed a respiratory phase shift. In normotensive animals, peak sympathetic nerve activity occurs in the post-I period, while in SHRs it occurs in late inspiration [6] [7], as shown in Figure 1.3.

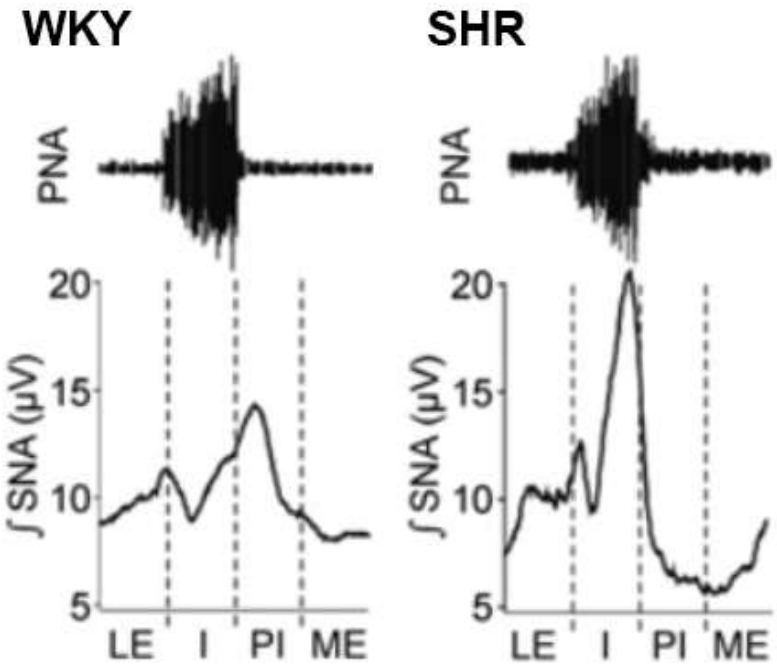

Figure 1.3: Altered respiratory-sympathetic coupling in SHR (right) compared to WKY (left), adapted from Simms et al. (2009) [7]. Respiratory-sympathetic bursts occur in the late inspiratory phase in the SHR (I), rather than the post-I phase (PI), as occurs in the WKY and other normotensive rat strains. LE: late expiration. ME: mid-expiration.

1.5 Project Aims

This project will investigate the source of altered respiratory-sympathetic coupling in the SHR, by comparing sympathetic, vagus, and phrenic nerve activities in SHR and their normotensive control strain, the Wistar Kyoto rat (WKY). While the time phase shift of peak sympathetic activity has been extensively studied in SHRs, vagal post-I activity has not been investigated. If dysfunction is due to phase-shifted activation of upstream post-I circuits (such as the KF or IRt), vagal post-I should also occur earlier in SHRs, during late inspiration instead of post-inspiration. However, if this does not occur, it suggests that sympathetic dysregulation in

hypertension is driven by a mechanism separate to vagal post-I, potentially amplified excitatory connections between preBötC and RVLM as previously suggested [13].

Optogenetic inhibition of the IRt will also be performed, as if IRt/KF overactivity is the cause of sympathetic dysregulation in hypertension, inhibition of this area should result in these effects being reversed and respiratory-sympathetic coupling should occur during the post-I period as it does with normotensive animals. As hypoxemia has previously been shown to stimulate vagal post-I activity, it will be used to assess how SHRs and WKYs respond to homeostatic challenge, and if post-I plays a role in this.

The role of vagal post-I activity in driving laryngeal adduction will be investigated using a novel method of filming larynx muscle movement, analysed with deep learning software. By integrating this data with simultaneously recorded diaphragm EMG, laryngeal adduction can be directly compared to respiratory phase. It is predicted that eliminating vagal post-I activity via optogenetic inhibition of the IRt will reduce or eliminate post-I laryngeal adduction.

2. Methods

2.1 Rats

Thirteen rats were used for experiments (6 SHR and 7 WKY, all of which were used for initial video recordings of laryngeal adduction). Electrophysiology was later performed on 9 of these animals (6 SHR and 3 WKY). An additional 6 rats were used for vector validation (2 SHR, 4 Long Evans), and 6 more were used for surgical training and practice injections (5 Long Evans, 1 Sprague Dawley). Animals weighed approximately 250g on arrival and reached 300-400g by the end of experiments.

Rats were supplied by the Animal Resource Centre, Western Australia. Animals were housed in groups of up to 3 in individually vented Techniplast cages in 12-12 hour light-dark cycles with food and water freely available. Experiments were approved by the Macquarie University Animal ethics committee (protocol 2018/024-20) and conducted in accordance with the Australian Code of Practice for the Care and Use of Animals for Scientific Purposes (2013), the NSW Animal Research Act (1985), and the NSW Animal Research Regulation (2021).

2.2 Video recordings of laryngeal adduction

Animals were anesthetised using a Darvall veterinary vaporiser, first in an induction chamber with 5% isoflurane in 1L/min oxygen, and then using a nose mask at ~2% isoflurane. Depth of anaesthesia was assessed with paw pinch and isoflurane modified to the minimum level required to maintain arreflexia. Atropine (Pfizer; 0.05mg/kg i.m.) was injected to reduce salivary secretions. The right abdomen was shaved, skin cleaned with 0.5% chlorhexidine, and an EMG hook electrode of 127µm diameter insulated steel wire was inserted into diaphragm using a 26 gauge needle by palpating the lower costal margin and insertion of the needle through the intercostal space from a lateral approach approximately 45^{o} towards the abdomen. Correct placement of recording electrodes was verified by the presences of bursting EMG in time with the inspiratory phase of the respiratory cycle.

To visualise the larynx, animals were suspended by the incisors from a wire frame made from a cake rack, with a small nose cone attached for anaesthesia (see Figure 2.1). A 100g weight was attached to lower jaw to keep the mouth open, and a cotton tip used to gently roll the tongue out of the mouth. A small clear plastic cone made from a Pasteur pipette, approximately 1.5 cm long, 1 cm diameter at the wide end with a 3 mm opening at the small end, was placed in the trachea using curved forceps to create a visual aperture. A flashing blue LED (50 ms, 1 Hz) was placed inside the mouth to allow for external calibration of video frame rate.

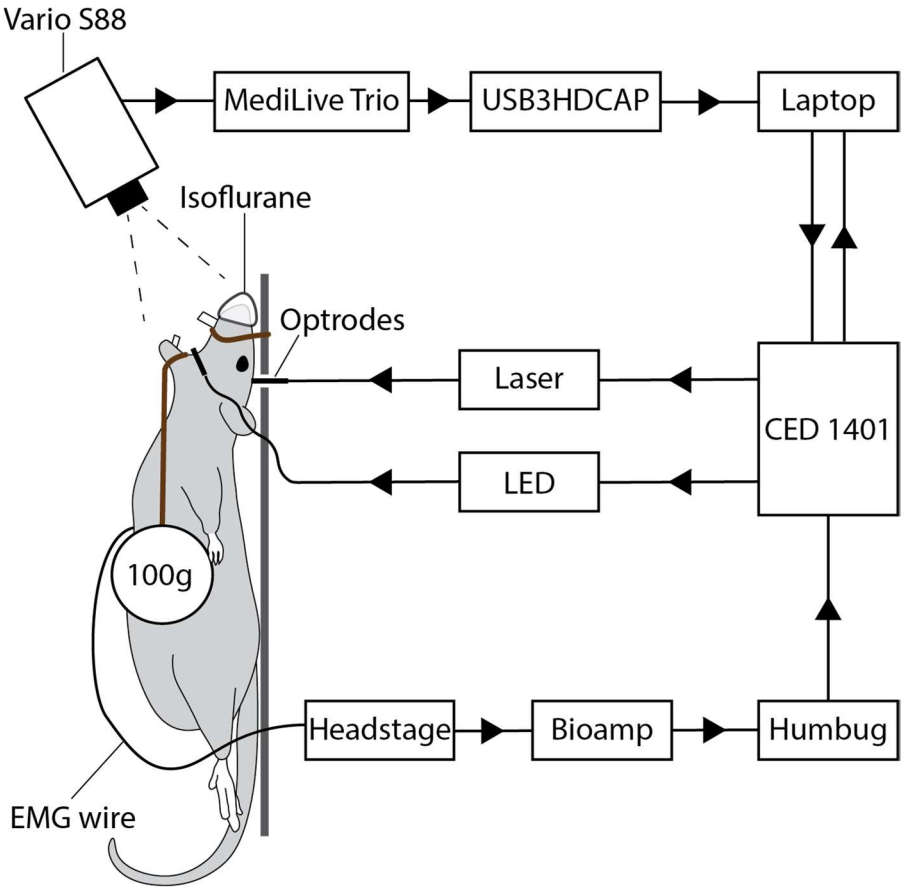

Figure 2.1: Experimental set up used for video recording of laryngeal adduction and diaphragm EMG

Recordings were sampled using Spike2 V10, with video capture coordinated by Spike2Video (Cambridge Electronic Design, UK). Video was captured using a Zeiss OPMI Vario S88 surgical microscope equipped with a MediLive Trio video camera console. The camera was connected to the computer via a StarTech USB3HDCAP video capture device.

EMG electrodes were connected to a CWE Super-Z headstage, a BMA-400 AC/DC bioamplifier (bandpass filter 100-3000 Hz), a Humbug noise eliminator, and then sampled by a CED Power1401 Mk II. Power1401 Mk II outputs were connected to a ThorLabs DC2100 LED, to drive the calibration light, and Laserglow 470 nm collimated diode laser to trigger optogenetic inhibition (Figure 2.1). Each recording lasted 2-5 minutes, and animals underwent several recording sessions before and after optrode implant surgery.

2.3 Electrophysiological recordings of respiratory, vagal, and sympathetic outputs

Rats were anesthetised with urethane (1.3g/kg i.p., diluted 10% w/v in saline), administered in 2 bolus half doses approximately 5-10 minutes apart. Depth of anaesthesia was assessed with withdrawal response to paw pinch. If required, additional top up of 10% of the original urethane dose was administered. Animals were shaved under the neck and along the left side of their back and abdomen.

The right jugular vein and right carotid artery were isolated and cannulated. The carotid cannula was connected to a transducer to measure arterial blood pressure throughout the experiment. The jugular vein was attached to a syringe pump for intravenous administration of drugs and saline as required. Tracheostomy was performed to allow for mechanical ventilation with O_2-enriched air. Once ventilated, animals were paralysed using cisatracurium (initial bolus dose 6mg/kg i.v., maintained by infusion at 14 mg/hr).

Throughout experiments, temperature was measured through a rectal probe and maintained at ~37°C with a heating pad. Arterial blood gas and electrolyse analysis (IDEXX VetStat) were performed periodically and ventilation adjusted to maintain pH ~7.4. End-tidal CO_2 was also measured using a Capstar-100. In cases of low pH or high CO_2, ventilation rate was increased, and vice versa. Some animals experienced low blood pressure due to blood loss from surgery, which was treated with an IV infusion of Hartmann's solution or physiological saline.

Cervical vagus nerves were bilaterally severed to allow recording of central respiratory activity without interference from afferent sensory signals such as lung stretch receptors and to desynchronise central respiratory rhythm from mechanical ventilation. The left vagus, phrenic, and splanchnic nerves were isolated, tied, and cut. Rats were secured in a stereotaxic frame and nerves loaded on to bipolar electrodes and submerged in paraffin oil. Neurograms were amplified, bandpass filtered (30-3000), and sampled at 3-5 ksamples/s using Spike2. Animals were allowed to stabilise for 5-10 minutes before beginning the experimental protocol. Animals were euthanised with Lethabarb (150mg/kg i.p.), perfused with heparin-saline then 4% paraformaldehyde, and brains removed.

2.4 IRt Inhibition

2.4.1 Vector Validation

Several vector validation surgeries were performed prior to the main series of experiments. The first vector, AAV-CAG-GTACR-P2A-mCherry (a gift from Professor Andrew Allen, University of Melbourne) was tested in 4 animals but resulted in weak reporter expression. Next we tried AAV-CkIIa-GTACR2-FusRed (AddGene) in 2 animals. This vector utilises the CaMKIIa promoter, which targets excitatory neurons [38], which was appropriate as neurons driving respiratory-sympathetic coupling in the IRt are thought to be excitatory [10, 11]. Vector validation of AAV-CkIIa-GTACR2-FusRed showed extensive labelling from 50 nL, 100 nL, and 200 nL injections (Figure 2.2). Due to the large amount of spread, it was decided to us 50 nL injections for subsequent experiments.

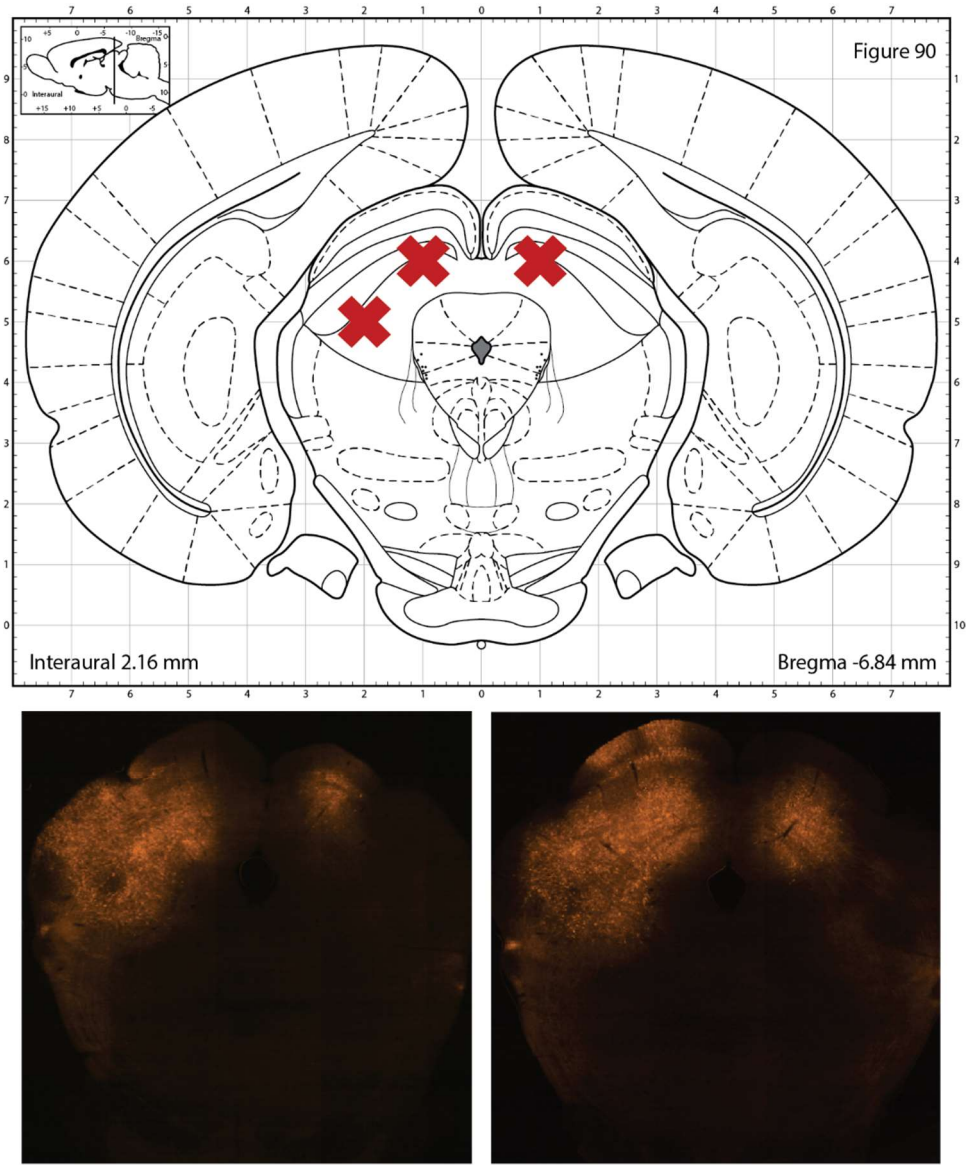

Figure 2.2: vector validation for AAV-CkIIa-GTACR2-FusRed. 200nL @ -2, 0.75, 5; 100nL @ -1, 0.75, 4; 50 nL @ 1, 0.75, 4. Top=target injection sites, bottom=vector expression in 2 rats

2.4.2 Vector Injections

Animals were anesthetised using a Darvall veterinary vaporiser, first in an induction chamber with 5% isoflurane in 1L/min oxygen, and then using a nose mask at ~2% isoflurane. Depth of anaesthesia was assessed with paw pinch and isoflurane modified to the minimum level required to maintain areflexia. Prophylactic antibiotic (cephalexin 100 mg/kg i.m.) and analgesic (carprofen 5mg/kg s.c.) drugs were administered and the top of head, neck, and left cheek were shaved, with care taken to avoid cutting whiskers, and skin cleaned with 2% chlorhexidine. Rat was placed in a stereotaxic frame (Neurostar Stereodrive) in skull-flat position, on a heating pad

maintained at ~37°C monitored via rectal probe. Local anaesthetic (bupivacaine 0.1 mL s.c.) was injected under the scalp at the incision site.

To target the IRt, left facial nucleus was mapped using antidromic field potentials evoked by stimulation of the facial nerve [39, 40]. A small incision was made in the left cheek, the facial nerve exposed, and stimulated with a bipolar electrode at 1-2 mA at a rate of 1 Hz. Visible whisker twitch confirmed that facial nerve stimulation was successful. The skull was exposed via scalp incision, and cleaned with hydrogen peroxide then saline solution. A rectangle section of bone approximately 1 mm wide was removed using a Dremel hand drill, 2mm lateral from Lambda, beginning at the lambdoid suture and extending caudally approximately 2mm. Dura was sliced with a 21g needle.

A glass pulled micropipette was loaded with 200µL of vector and a platinum wire electrode. The pipette was inserted into brain at 2 mm lateral and 2 mm caudal from Lambda and gradually lowered while observing the field potential on an oscilloscope. Upon encountering a confirmed facial field potential the pipette withdrawn and moved 300 µm caudal until responses were no longer seen, signifying the caudal boundary of the facial nucleus. The most caudal track with a visible facial field potential was determined the ‘facial pole’ and this was used as the rostro-caudal coordinate for IRt injections. Injection depth was calculated as 350µm above the most dorsal point at which a field potential was found (across all tracks in for individual animal), 1.75mm lateral from midline (Figure 2.3).

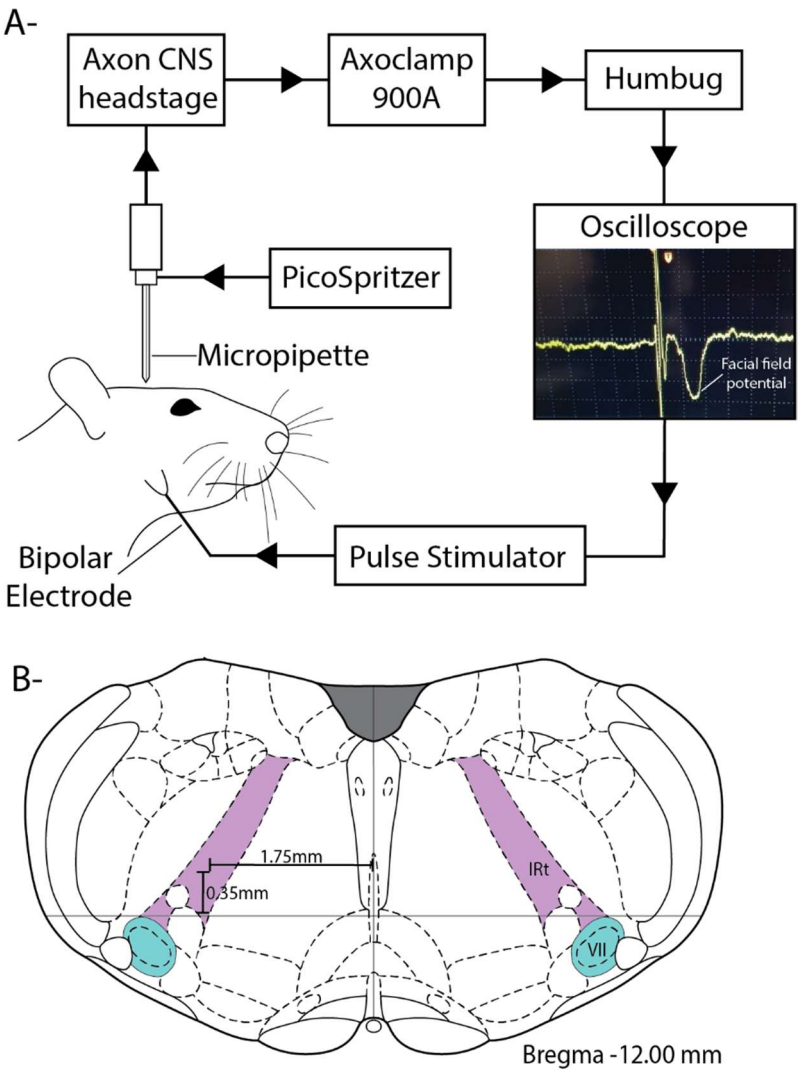

Figure 2.3: Method for facial nucleus mapping to target IRt injections. A- experimental set up, including example of antidromic facial field potential seen on oscilloscope. B- location of target injection site (purple) relative to facial nucleus (blue). IRt= intermediate reticular nucleus, VII= facial nucleus.

50 nL of vector was injected slowly over 5 minutes using a Picospritzer III, then left for an additional 5 minutes before slowly withdrawing the pipette. Injection was repeated on the right side, using the same coordinates through a small hole drilled in the skull.

Following vector injections, 12 mm long optrodes were implanted, targeting the same coordinates as injection sites (although 300 µm dorsal) and secured with a small amount of super glue (UHU) then built up with dental cement (Densply Rapid Repair). Animals were monitored closely after surgery, and given a minimum of 3 weeks to recover before performing further experiments.

2.4.3 Hypoxic Challenge

During nerve recordings with IRt inhibition, hypoxemia was also induced (see section 2.4.4 below). This involved turning off supplemental oxygen for a period of 1 minute, during this time animal was breathing room air only. This approach was based on a technique previously validated by this group [11], which showed a drop in arterial PO2 from ~500 to ~60 mmHG in ventilated urethane anesthetised animals.

2.4.4 Inhibition Protocol

Ferrules were cleaned with ethanol swab, sprayed with WD-40, and attached to optical patch cables with ceramic sleeves. Cables were connected to a blue laser by a double rotary joint or split optic cable. Laser intensity was calibrated at 5 mV per channel using a Thorlabs optical power metre. Inhibition experiments were performed as per the protocol outlined below.

Larynx Videos

- 1 min baseline activity
- 10 sec inhibition
- 1 min recovery

Electrophysiology

- 5 min baseline activity
- 1 min inhibition
- 5 min recovery
- 1 min inhibition (repeat)
- 5 min recovery
- 1 min hypoxemia
- 5 min recovery
- 1 min hypoxemia with inhibition
- 5 min recovery

2.5 Imaging

After perfusion, brains were immersed in paraformaldehyde (PFA) for a minimum of 24 hours, then stored in phosphate-buffered saline (PBS). Medulla was sliced into 50µm coronal sections on a Leica VT1200s vibratome and separated into 4 pots. 1 pot was mounted immediately, in order, on glass microscope slides with DAPI mounting medium (Dako) and air

dried for 24 hours. Sections were imaged on a Zeiss AxioImager fluorescence microscope at 10x resolution using AlexaFluor channel 555 to visualise FusRed expressed in injection sites, and AlexaFluor channel 350 to visualise DAPI in cell nuclei.

2.6 Data Analysis

2.6.1 Tracking laryngeal adduction with Deep Lab Cut

Larynx videos were annotated using Deep Lab Cut software (DLC) [41] . The algorithm was trained based on manually annotated fames from 25 videos, with a minimum of 20 frames per video. Frames for manual annotation were extracted based on kmeans clustering. Figure 2.4 illustrates how frames were labelled: 11 points were labelled in each frame; 5 points on the margin of each laryngeal fold, and 1 point representing the point of fusion of the two laryngeal folds (“apex”).

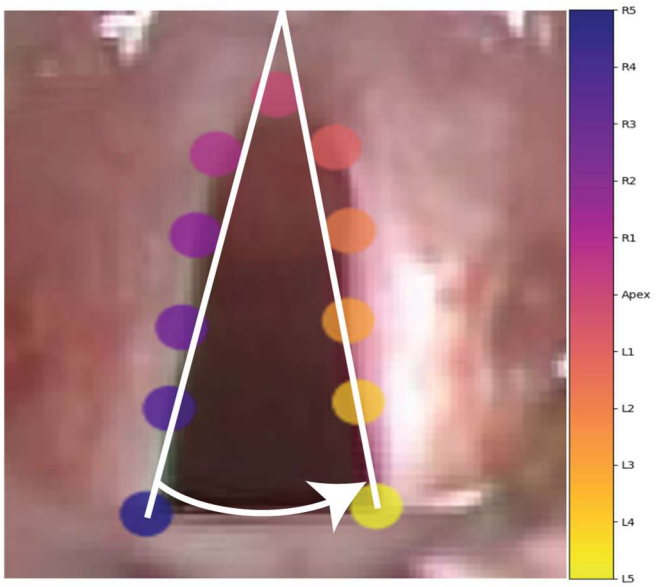

Figure 2.4: Frame of larynx video with points manually labelled, showing lines of best fit and angle of intersect.

DLC predicts the pixel co-ordinates of each label per frame, and creates an output file listing the X and Y coordinates of each marker in each frame of the video (0,0 is top left corner), along with a probability value for each point. Analysis was deemed successful when probability was greater than 0.9. In cases where probability was lower, frames with poor labelling were manually selected, relabelled, training repeated, and video reanalysed.

Data was then imported into Microsoft Excel. Lines of best fit were calculated for left and right laryngeal margins using the following formula (both sides included the Apex), where X is the line through the left margin and Y describes the line through the right margin.

$$\bar{X} = \frac{x_A + x_{L1} + x_{L2} + x_{L3} + x_{L4} + x_{L5}}{6}$$

$$\bar{Y} = \frac{y_A + y_{L1} + y_{L2} + y_{L3} + y_{L4} + y_{L5}}{6}$$

$$m = \frac{\sum(x_i - \bar{X})(y_i - \bar{Y})}{\sum(x_i - \bar{X})^2}$$

$\bar{X} = mean\ x$

$\bar{Y} = mean\ y$

$m = slope$

Laryngeal adduction was approximated by measuring increases in the angle of the intersect, calculated using the formula below:

$$tan = \frac{m_L - m_R}{1 + (m_L \times m_R)}$$

$$degrees = tan^{-1}(tan)$$

As this equation calculates the smallest angle of intersect between the two lines, when the larynx opens more than 90 degrees the equation 'flips' to the opposite angle, and the number becomes negative (as illustrated in Figure 2.5 below).

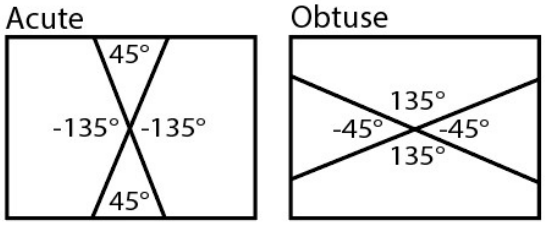

Figure 2.5: Example of angle calculation for acute (<90°) and obtuse (>90°) angles. For acute angles the value given by the above equation reflects the angle of the larynx. For obtuse angles, the equation reports the opposite angle as a negative number.

This is corrected by Excel's IF function, which reports the original angle if the value is above zero, and adds 180° to negative values to correct obtuse angles (e.g. -45+180=135).

$$corrected\ angle = IF(angle > 0, angle, 180 + angle)$$

2.6.2 Alignment of video and EMG data

A flashing LED light illuminated a portion of the field of view to enable video frame calibration. Proper alignment of this data is essential for accurate triggering of laryngeal angle relative to diaphragmatic activity. Tracker software (Physlets) was used to extract blue signal intensity for each frame of the video, exported frame-by-frame into spreadsheets that would later be compared to trigger time in Spike2 to identify any delay or drift in framerate.

While DLC and Tracker both provide one data point per video frame (approx. 60 Hz), diaphragm EMG signal has a much higher sampling rate. EMG data was downsampled and exported from Spike2 at 1000 Hz. EMG data (and timestamps from the Spike2 file) were imported into Excel, as were the timestamps, derived laryngeal angle, and blue light intensity values from simultaneously recorded videos. The Excel Closest Match function was used to align video data with corresponding Spike-generated time stamps (this essentially takes each time point for EMG data, compares it with the timestamp of each frame, finds the closest frame, and populates each cell with the relevant larynx angle or blue value) and interpolates missing datapoints from the video frames (to compensate for the lower sampling frequency of video data). Data was then imported back in to Spike2 for further analysis.

2.6.3 Cycle-triggered averaging of laryngeal angle

Larynx videos were performed in each animal before and after vector injection surgery. For comparison between baseline SHR and WKY activity, the best recording from each animal was selected. This was determined by visualisation of the larynx, successful DLC tracking, and quality of EMG trace. A period of 10 respiratory cycles was selected for analysis for each video,

ranging from 8-15 seconds long, depending on individual respiration rate. For IRt inhibition experiments, data was separated into 3 epochs 10 seconds before, during, and after inhibition.

Larynx angle traces were smoothed (t=0.05) and differentiated (dangle/dt, t=0.05) to reduce noise and highlight change in larynx angle over time. Onset and offset of diaphragm EMG activity were marked as events on the trace using the falling/rising envelopes of rectified smoothed EMG and used to calculate inspiration time (TI), expiration time (TE), and total respiratory cycle length (Ttotal). Diaphragm-triggered waveform averages were created for raw larynx angle and dangle/dt. Post-I laryngeal adduction time was quantified as the time of peak laryngeal adduction (indicated by slope) relative to time of EMG off.

2.6.4 Electrophysiological recordings of phrenic, vagal, and sympathetic activities

Waveforms for phrenic nerve activity (PNA), vagus nerve activity (VNA) and sympathetic activity (SNA) were rectified and smoothed (t=50ms). Onset and offset of phrenic nerve activity were captured as event marker channels, to calculate respiratory phase timing (TI, TE, Ttot) using the same method as described above for diaphragm EMG.

Phrenic-triggered waveform averages were generated for 60 seconds of PNA, VNA, and SNA activity, to identify differences in vagus and sympathetic post-I activity between SHRs and WKYs. For IRt inhibition, data was separated into 3 epochs of 60 seconds before, during, and after inhibition. For hypoxemia experiments, data was separated into 7 epochs of 15 seconds duration, which represented 15 seconds before hypoxemia, 1 minute during hypoxemia, and 30 seconds after hypoxemia. Hypoxemic trials were separated into more epochs of shorter duration to better capture the gradual changes seen across period of hypoxic challenge and during recovery. Conversely, the effect of optogenetic inhibition is instant, and immediately reversed once laser is turned off. Due to this, IRt inhibition was separated into 3 epochs only, capturing the periods before, during, and after inhibition.

Time of post-I activity was measured as the time of peak VNA/SNA activity relative to the end of inspiration, identified as the mid-point between peak and trough phrenic nerve

activity. This was reported as an average value for each epoch. Arterial blood pressure was measured continually through electrophysiology experiments. Maximum systolic and minimum diastolic blood pressure were quantified for each epoch.

2.6.5 Statistical tests

For video experiments, time of laryngeal adduction, relative to the end of inspiration, and respiratory phase duration were compared between WKY and SHR using two-tailed unpaired t-tests (Welch corrected due to unequal variances).

For electrophysiology experiments, time of peak vagal and sympathetic activity, relative to the end of inspiration, was compared between WKY and SHR using two-tailed unpaired t-tests. A mixed effects analysis (REML) with multiple comparisons was used to compare effect of hypoxemia on peak sympathetic and vagal post-I time (relative to end of inspiration) between WKY and SHR. Ideally ANOVA would have been used, but this was not possible due to missing data for epochs 6 and 7 in 1 WKY.

Respiratory phase duration (TI, TE, and Ttot) were compared at baseline between WKY and SHR using two-tailed unpaired t-tests. Change in TI, TE, and Ttot throughout hypoxemia was compared between WKY and SHR using mixed effects analysis (REML) with multiple comparisons. Changes in arterial blood pressure in response to hypoxemia were compared between WKY and SHR using two-way repeated measures ANOVA with multiple comparisons, with epochs 6 and 7 excluded from analysis.

To determine the effect of IRt inhibition on electrophysiological parameters, values before, during, and after inhibition were compared using 4 instances of inhibition in the same animal. One-way repeated measures ANOVAs with multiple comparisons were used to assess amplitude of vagal and sympathetic post-I activity, time of peak vagal and sympathetic activity, relative to the end of inspiration, respiratory phase duration (TI, TE, Ttot) and arterial blood pressure.

Experiments investigating the effects of IRt inhibition on post-I activity and respiratory phase timing over the course of hypoxemia only consisted of 1 trial under each condition, in a single animal, so further statistical analysis was not appropriate for this dataset.

3. Results:

3.1 Video recording of laryngeal adduction

3.1.1 Larynx Activity

Videos were selected based on quality of EMG trace, visibility of larynx in frame, and DLC tracking performance. The best recording session for each animal was used, for a total of 7 WKYs and 6 SHRs (total n=13). Of these recordings, 6 were recorded before vector injection/optrode implant surgery (WKY=4, SHR=2), and 7 were recorded after surgery (WKY=3, SHR=4). Figure 3.1 below shows video frames at different times of the respiratory cycle, overlaid with DLC labels, and corresponding Spike2 recordings from the same experiments showing laryngeal angle derived from video data (differentiated and raw) integrated with simultaneously recorded diaphragm EMG.

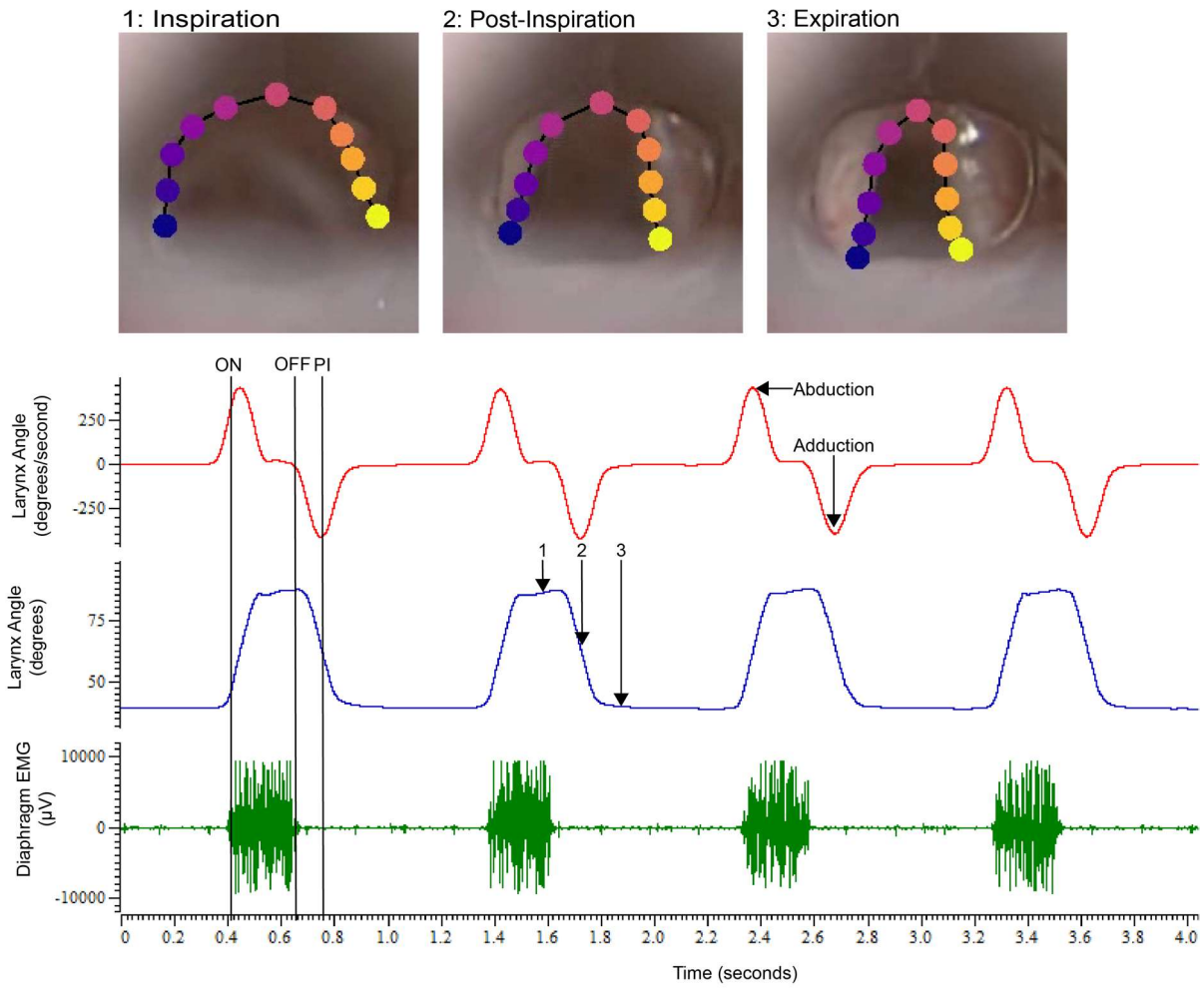

Figure 3.1: Example of larynx video frames labelled by Deep Lab Cut (top panels) and example of differentiated (top trace) and raw (middle trace) larynx angle plotted on the same timescale as diaphragm EMG (lower trace) ON= EMG on, beginning of inspiration, OFF= EMG off, end of inspiration, PI= post-I laryngeal adduction, 1=inspiration, 2=post-inspiration 3=expiration

10 of the 13 individuals had a similar pattern of activity shown in Figure 3.1, characterised by laryngeal abduction at the onset of diaphragm EMG activity (i.e. the onset of inspiration), indicated by a positive inflection on the differentiated trace, and adduction at the end of diaphragm EMG activity (i.e. the start of the post-inspiratory period), indicated by a negative inflection on the differentiated trace. Speed of adduction (measured in degrees per second) peaked during the post-I period. Of the 3 rats excluded from analysis, 2 had abnormal waveforms due to poor DLC tracking. The third had an abnormal pattern of activity, with a small adduction occurring in the post-I period lasting 30-100ms, with the larynx remaining abducted throughout the rest of the respiratory cycle.

Of the waveform averages shown in Figure 3.2 A-C below, the minimum angle during adduction was 30°, and the maximum during abduction was 92°. Range of movement between adduction and abduction varied from up to 58° to as little at 10°. Mean time of peak post-I laryngeal adduction was 0.082 ± 0.035 seconds after EMGoff for WKYs, and 0.068 ± 0.068 seconds for SHRs (see Figure 3.2 D). A two-tailed unpaired t-test (Welch corrected) did not find a statistically significant difference in the timing of laryngeal adduction with reference to the end of inspiration between the two groups ($t=0.18$, $p=0.86$).

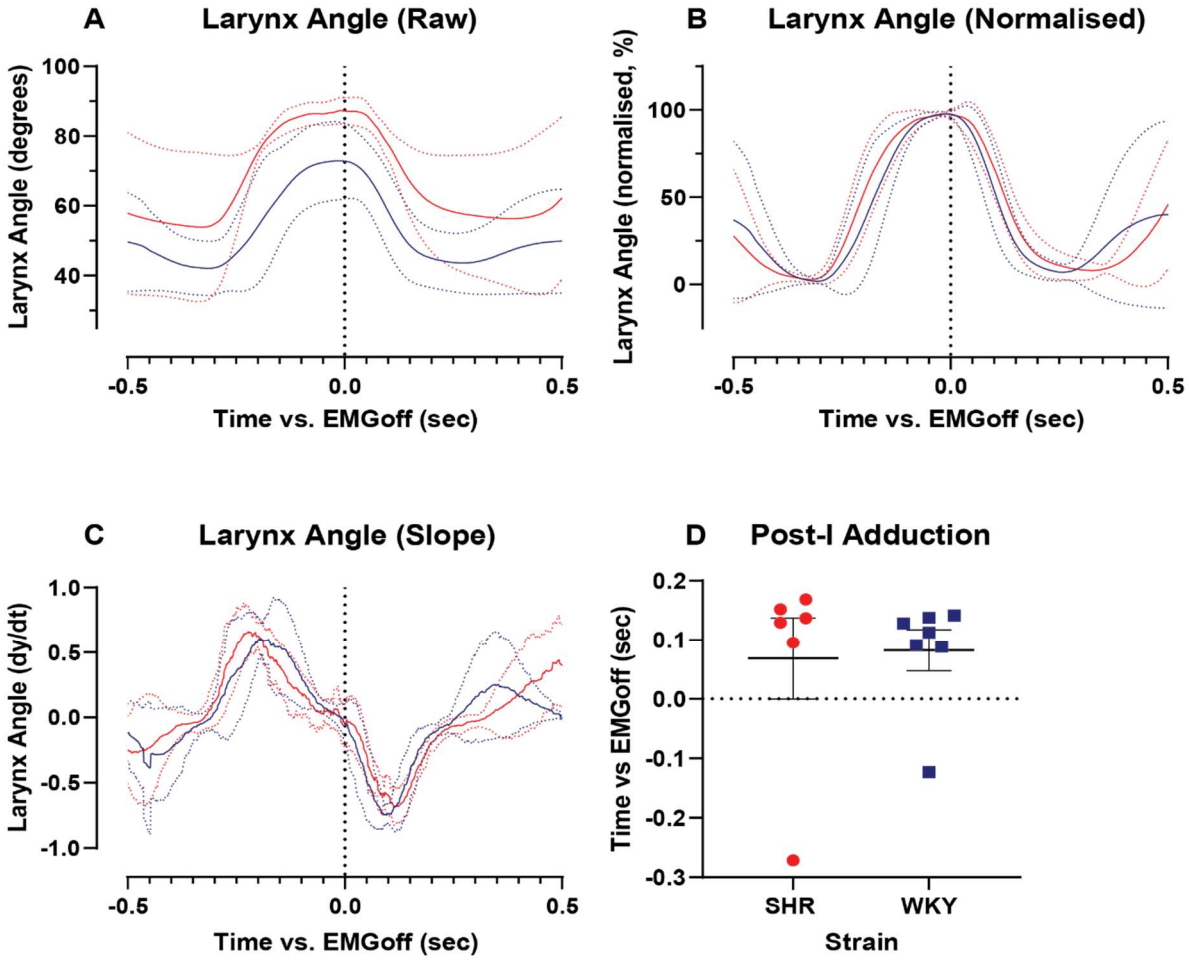

Figure 3.2 A-C: Larynx angle waveform averages for WKY (blue) and SHR (red) rats. A: Raw waveforms (dotted lines indicate SEM) B: the same data normalised between 100 % (maximum angle) and 0% (minimum angle) C: the same data normalised and differentiated: negative deflections indicate adduction, positive indicated abduction. D: time of peak laryngeal adduction from end of inspiration, measured from slope deflection, with SEM.

We conclude that there is no significant difference in timing of post-I laryngeal adduction between SHR and WKY rats under light isoflurane anaesthesia.

3.1.2 Respiratory Phase Timing

Respiratory phase timing was measured from EMG activity recorded simultaneously with larynx videos. Inspiration time (TI), expiration time (TE), and total respiratory cycle length (Ttot) were quantified and are presented in Figure 3.3. Two-tailed unpaired t-test (Welch corrected) found no significant difference in TI, TE, or Ttot between SHR and WKY rats.

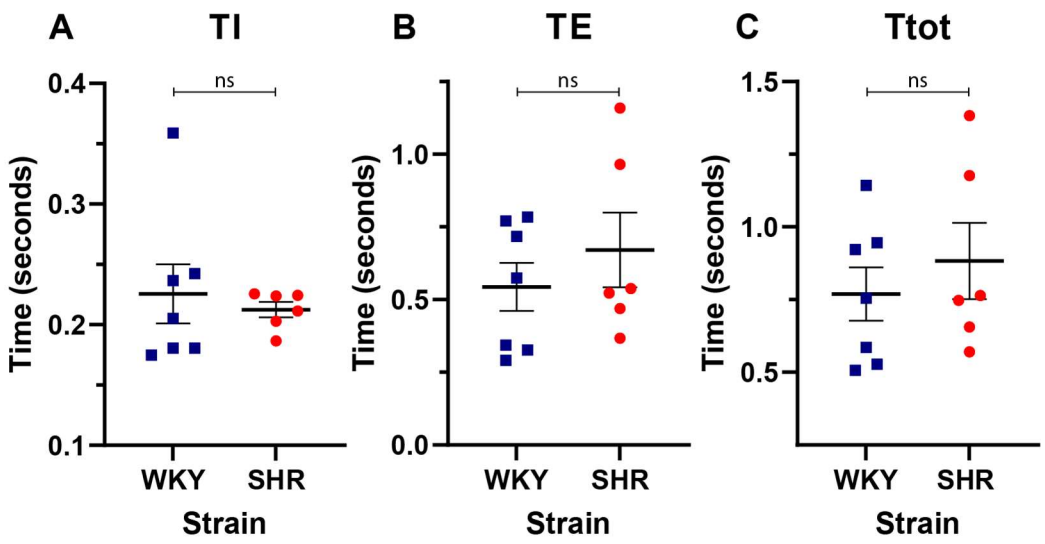

Figure 3.3: Respiratory phase timing derived from diaphragm EMG activity. TI=inspiration time (A), TE=expiration time (B), Ttot=total respiratory cycle length (C) Blue square=WKY, red circle=SHR

Based on these results, there does not appear to be any difference in respiratory phase timing between SHR and WKY rats under light isoflurane anaesthesia.

3.2 Electrophysiological recordings of post-I vagal and sympathetic activities in WKY and SHR

3.2.1 Baseline respiratory parameters

Of the 13 rats used for video experiments, electrophysiological recordings were successfully performed on 9 (6 SHR, 3 WKY). An example of traces obtained from electrophysiology experiments is shown below in Figure 3.4.

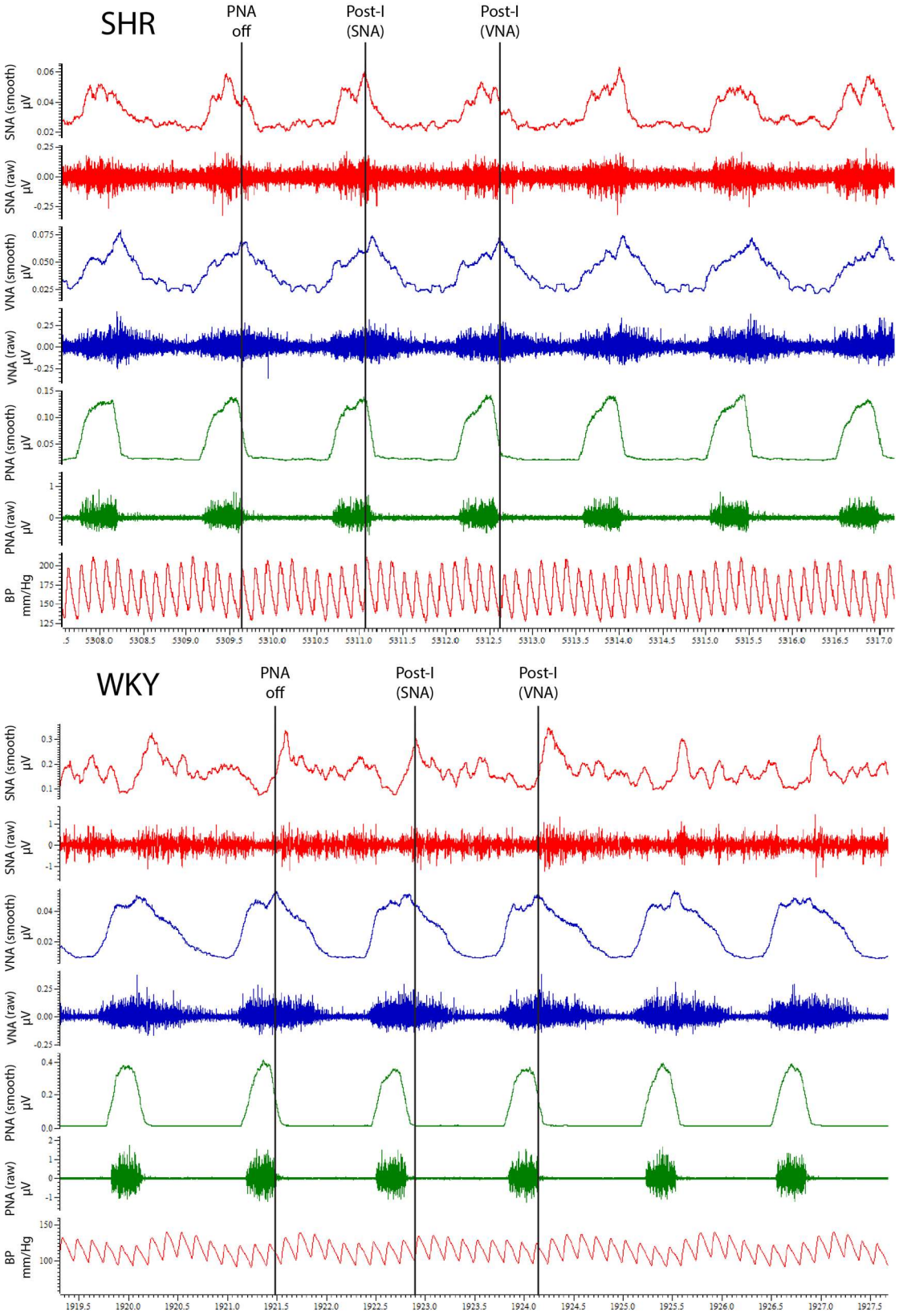

Figure 3.4: Examples of raw and smoothed traces of SNA (red, top trace), VNA (blue), PNA (green) and AP (red, bottom trace) recordings obtained from electrophysiology experiments in SHR (top) and WKY rats (bottom). SNA=sympathetic nerve activity, VNA=vagus nerve activity, PNA=phrenic nerve activity, AP=arterial blood pressure

3.2.2 Vagal and sympathetic post-I activity in WKY and SHR

Phenic-triggered waveform averages were created from 60 second blocks of data to determine time of post-I vagus (VNA) and sympathetic nerve activities (SNA) relative to the end of inspiration (indicated by PNAoff), as shown in Figure 3.5.

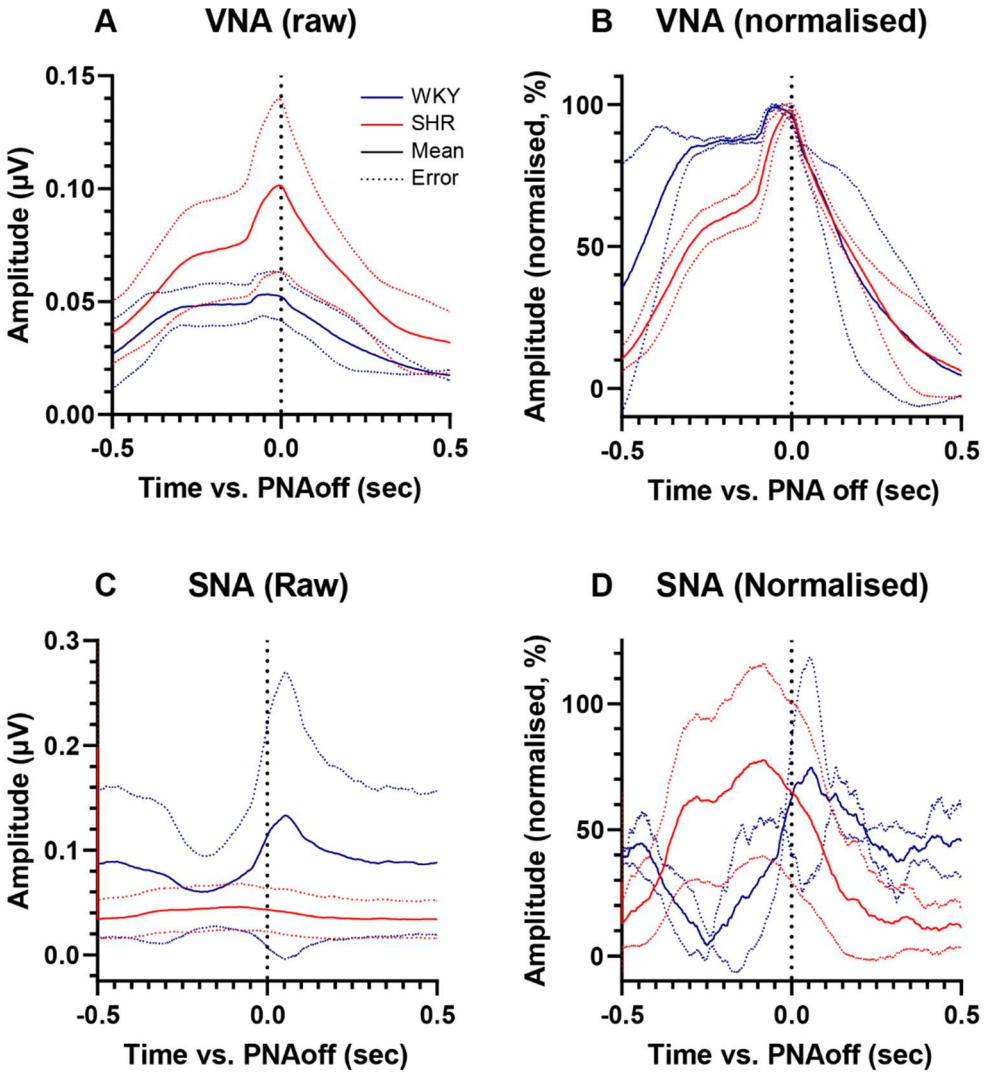

Figure 3.5: Phrenic-triggered waveform averages of baseline vagus (A, B) and phrenic (C, D) nerve activity, raw (A,C) and normalised (B,D), obtained from 60 seconds of baseline activity. Blue=WKY, Red=SHR, solid line=mean, dotted line=SEM. VNA- vagus nerve activity, SNA=sympathetic nerve activity.

As previously reported, respiratory-sympathetic coupling in the SHR occurred earlier in the SHR than the WKY, with sympathetic bursts manifesting in the inspiratory period rather than the post-I phase, as seen in the WKY (-0.025 ± 0.021 vs. 0.11 ± 0.018, SHR vs. WKY respectively, two-tailed unpaired T test P = 0.0044, Figure 3.5 C & D, Figure 3.6 B). In contrast, we found no evidence for similar phase-shifting of post-I vagal activity in the SHR; if anything,

vagus post-I activity occurred earlier in WKYs than SHRs (0.023 ± 0.006 vs. -0.0014 ± 0.01 s, p=0.071, Figure 3.5 A & B, Figure 3.6A).

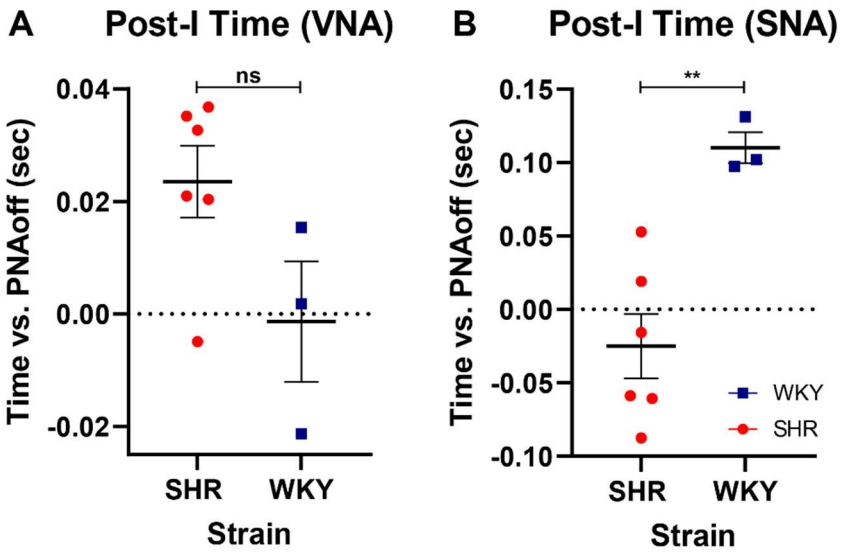

*Figure 3.6: Time of peak post-I vagal (VNA, A) and sympathetic activity (SNA, B) derived from phrenic-triggered waveform averages. **=p<0.01, ns=not significant.*

3.2.3 Responsiveness of post-I activity to acute hypoxemia

VNA and SNA post-I time were also measured before, during, and after 1 minute of hypoxemia (see Figure 3.7). Mixed-effects analysis (REML) with multiple comparisons was performed to determine if SHR and WKY rats had a different post-I responses to low oxygen levels.

For VNA post-I time (Figure 3.7 A), mixed effects analysis found significant effects for Epoch ($F(6,34)=10.73$, $p=<0.0001$), strain ($F(1,6)=75.19$, $p=0.0001$), and an interaction between epoch and strain ($F(6,34=12.45$, $p=<0.0001$), suggesting differential responsiveness to this stimulus. While SHR post-I time remained stable throughout the protocol, WKY had a small decrease during hypoxemia, followed by a larger decrease in recovery period before returning to baseline. Multiple comparisons found that for WKYs, Epoch 6 had significantly earlier post-I time than Epoch 1 ($p=<0.0001$).

For SNA post-I time (Figure 3.7 B), SHRs showed a steady increase in post-I time during hypoxemia, followed by a decrease during recovery. WKY did not appear to have any consistent pattern. Mixed effects analysis found a significant interaction effect between strain and epoch

(F(6,40)=3.14, p=0.013) but no effect for Epoch (F(2.99, 19.97)=1.23, p=0.33) or strain (F(1,7)=1.22, p=0.31) alone.

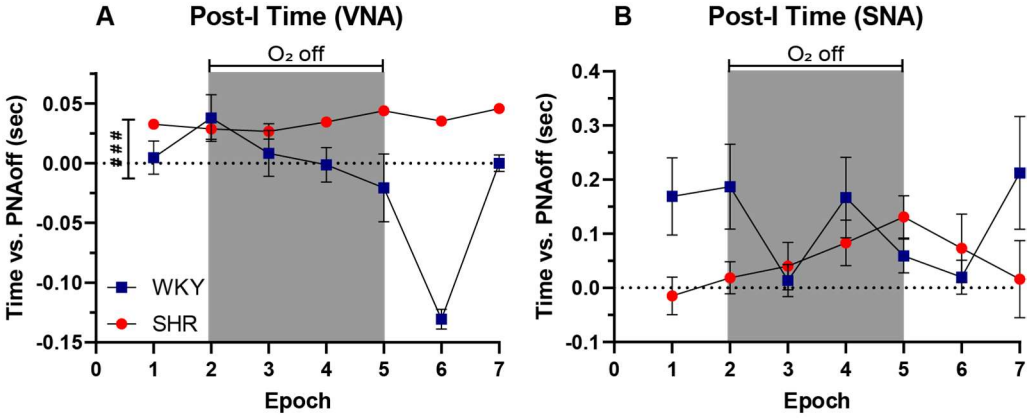

Figure 3.7: Time of peak post-I activity in SHR and WKY rats before, during and after hypoxemia. VNA=vagus nerve activity SNA=sympathetic nerve activity PNA=phrenic nerve activity ### = p<0.0001 (mixed effects ANOVA)

3.2.4 Respiratory phase timing

Inspiration time (TI), expiration time (TE), and total respiratory cycle length (Ttot) were obtained from PNAon and PNAoff time, as indicated in Figure 3.8. As was the case with recordings conducted under isoflurane, at baseline (Epoch 1, Figure 3.8), two-tailed unpaired t-test did not find any significant difference between SHR and WKY for TI (p=0.43), TE (p=0.29), or Ttot (p=0.5846).

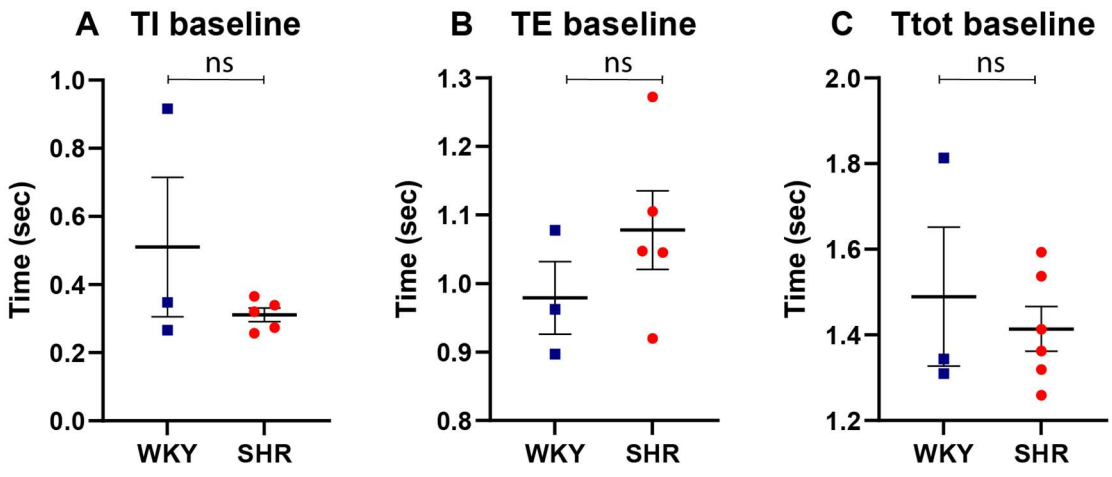

Figure 3.8 A: Inspiration time (TI), B: expiration time (TE), and C: total respiratory cycle length (Ttot) for WKY and SHR groups at baseline (Epoch 1), derived from phrenic nerve activity. ns=p>0.05 error bars=SEM

Over hypoxemia both WKY and SHRs increased their respiratory rate (evidenced by a reduction in cycle length, Ttot), followed by a rebound prolongation of Ttot (i.e. post-hypoxic

frequency decline, Figure 3.9 C). SHR had slightly shorter cycle duration than WKY throughout hypoxemia, which increased immediately after hypoxemia. Mixed-effects analysis (REML) with multiple comparisons found a significant effect for Epoch ($F(6,40)=6.15$, $p=<0.0001$) and an interaction between Epoch and strain ($F(6,40)=3.62$, $p=0.006$), but no effect for strain alone ($F(1.7)=0.004$, $p=0.95$). Multiple comparisons found that compared to Epoch 1, SHRs had significantly lower Ttot at Epoch 4 ($p=0.023$) and significantly higher Ttot at Epoch 7 ($p=<0.0001$). All multiple comparisons for WKY were non-significant.

The effect of hypoxemia on respiratory cycle frequency was evoked by a reduction in TE, with no effect seen on TI. Mixed-effects analysis (REML) with multiple comparisons found a significant effect for Epoch ($F(6,34)=6.45$, $p=0.0001$) and a significant interaction between Epoch and strain ($F(6,34)=4.52$, $p=0.0018$), with SHRs having significantly longer TE during Epoch 7 ($p=0.017$) compared to WKYs. No effect was found for strain alone ($F(6,34)=6.45$, $p=0.093$).

In contrast, there was no significant difference in TI between WKY and SHRs throughout the hypoxemia protocol (Figure 3.9 A). Mixed-effects analysis (REML) with multiple comparisons of TI found a significant effect for Epoch ($F(6,34)=4.13$, $p=0.0032$) but not for strain ($F(1,6)=2.44$, $p=0.17$) and no interaction between strain and Epoch ($F(6,34)=1.46$, $p=0.22$). Multiple comparisons were performed comparing each Epoch to Epoch 1. WKYs had no significant change in TI compared to baseline, but SHRs had significantly lower TI at Epoch 4 ($p=0.023$), Epoch 5 ($p=0.003$), and Epoch 6 ($p=0.007$), compared to Epoch 1.

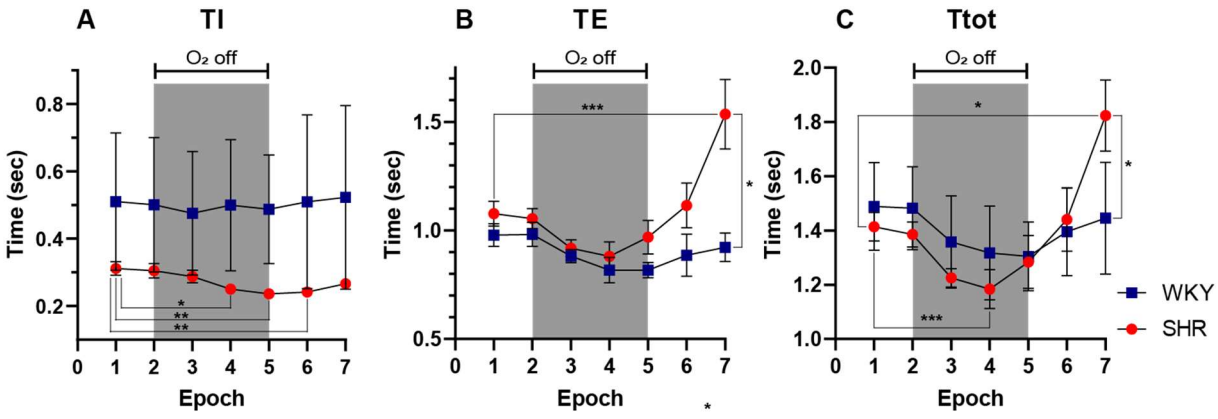

*Figure 3.9: Duration of inspiration (A), expiration (B), and respiratory cycle length (C) in WKY and SHR before, during, and after hypoxemia. *=p<0.05, **=p<0.01, ***p=<0.001*

3.2.4 Blood pressure

Systolic and diastolic arterial blood pressure (AP) were measured for each epoch to assess differences in response to hypoxemia between SHR and WKY rats. While both strains showed an increase in blood pressure during hypoxemia, this effect was more pronounced in SHRs (see Figure 3.10)

SHR had significantly higher systolic (p=<0.0001) and diastolic (p=<0.0001) AP than WKY throughout the experiment, as expected. Due to missing values in Epochs 6 and 7, two-way repeated measures ANOVA with multiple comparisons was performed on systolic and diastolic AP for Epochs 1-5 only. For systolic AP, a significant effect was found for epoch ($F(4,28)=0.306$, $p=0.03$), but not for strain ($F(1,7)=4.151$, $p=0.081$) or an interaction between Epoch and strain ($F(4,28=0.089)$, $p=0.48$). No significant effects were found for diastolic AP.

Multiple comparisons found that, compared to Epoch 1, SHR had higher systolic AP at Epochs 4 ($p=0.046$) and 5 ($p=0.0043$), while WKYs did not ($p=0.88$ and $p=0.96$ respectively). SHRs also had higher diastolic blood pressure at Epoch 5 compared to Epoch 1 ($p=0.018$).

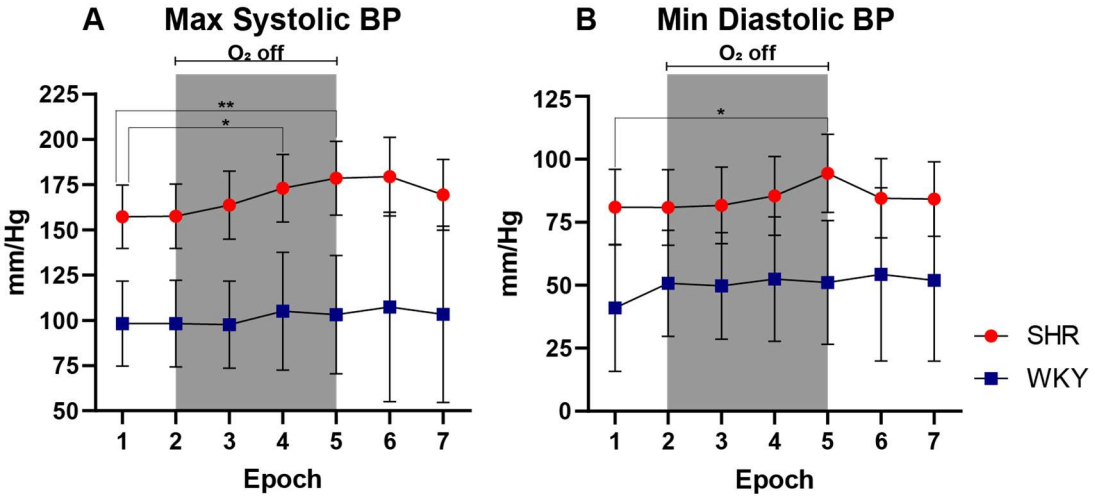

*Figure 3.10: Systolic (A) and diastolic (B) arterial blood pressure for SHR and WKY rats before, during, and after hypoxemia. *=p<0.05, **=p<0.01.*

3.3 Optogenetic IRt Inhibition

3.3.1 Injection Sites

Physiological responses to IRt inhibition were only observed in 1 animal (SHR). This animal showed extensive reporter labelling throughout the IRt, as shown in Figure 3.11 A. Labelling was also seen in nearby regions including the parvocellular reticular nucleus (PCRt), the nucleus ambiguus (NA) and Bötzinger complex (BötC). In all other cases injections were off-target, typically dorsal to the IRt with reporter expression concentrated in the solitary tract (see Figure 3.11 B-D). Data from the single animal with an on-target injection are considered below.

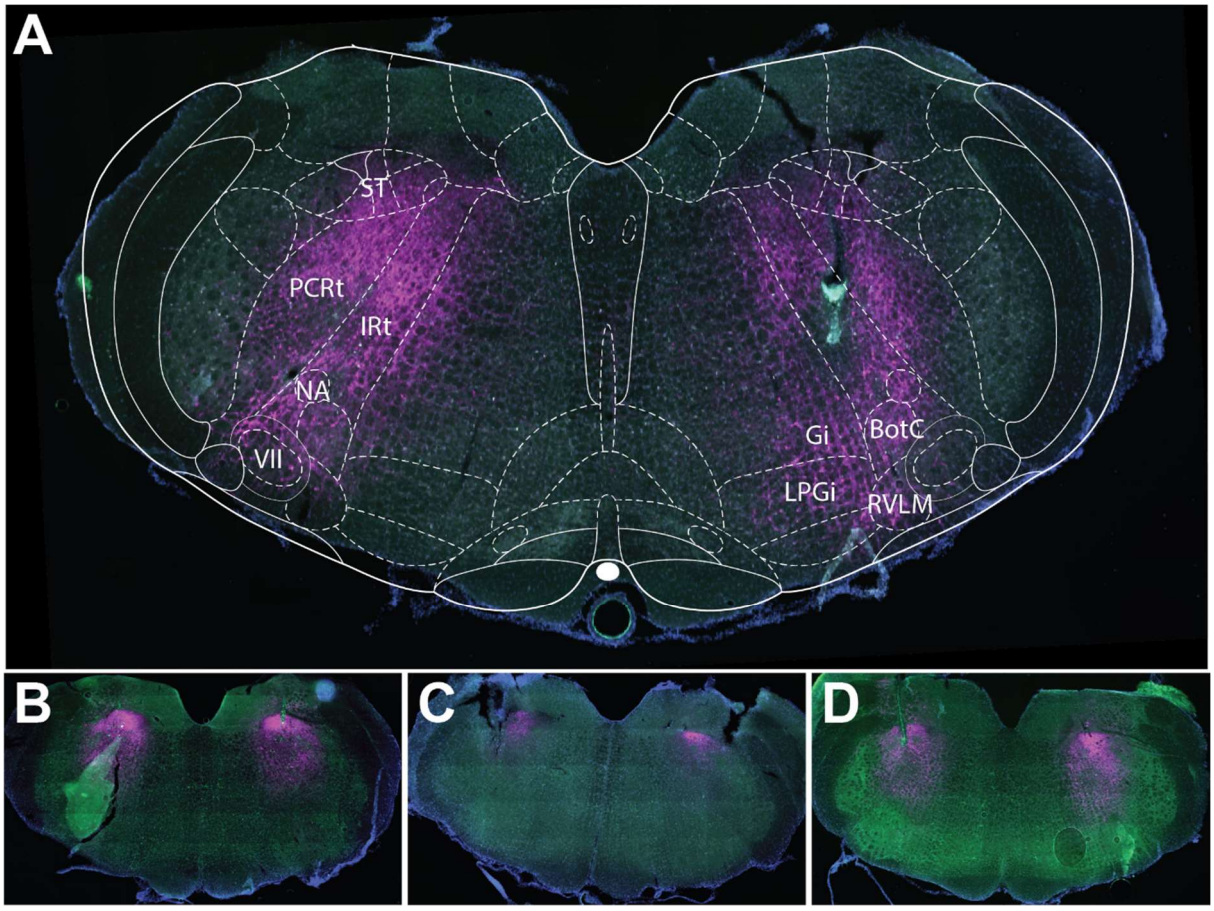

Figure 3.11: Injection site of responder (A: note optrode track on the RHS), and typical examples of off-target injections in rats in which no physiological responses were seen to IRt inhibition (B-D). Magenta indicates cell bodies expressing GtACR. IRt=intermediate reticular nucleus PCRt=parvocellular reticular nucleus NA=nucleus ambiguus VII=facial nucleus ST= solitary tract Gi= gigantocellular reticular nucleus LPGi=lateral paragigantocellular nucleus BötC=Bötzinger complex RVLM=rostral ventrolateral medulla

3.3.2 Larynx Activity

Figure 3.12 shows the effect of IRt inhibition on laryngeal adduction videography in the responsive animal. Diaphragm-triggered waveform averages of larynx angle and slope were plotted for data 10 seconds before, during, and after bilateral IRt inhibition. Under isoflurane anaesthesia, IRt inhibition reduced laryngeal angle at all phases of the respiratory cycle but did not abolish respiratory control of largyngeal constriction (Figure 3.12 A).

The slope of waveform average was not significantly affected by inhibition (Figure 3.12 B), indicating that while the extent of laryngeal movement decreased, the overall pattern of activity did not change. Interestingly, the effect of inhibition was not sustained, as shown by waveforms in Figure 3.12; activity partially recovered during inhibition, then overshot baseline when the laser was turned off.

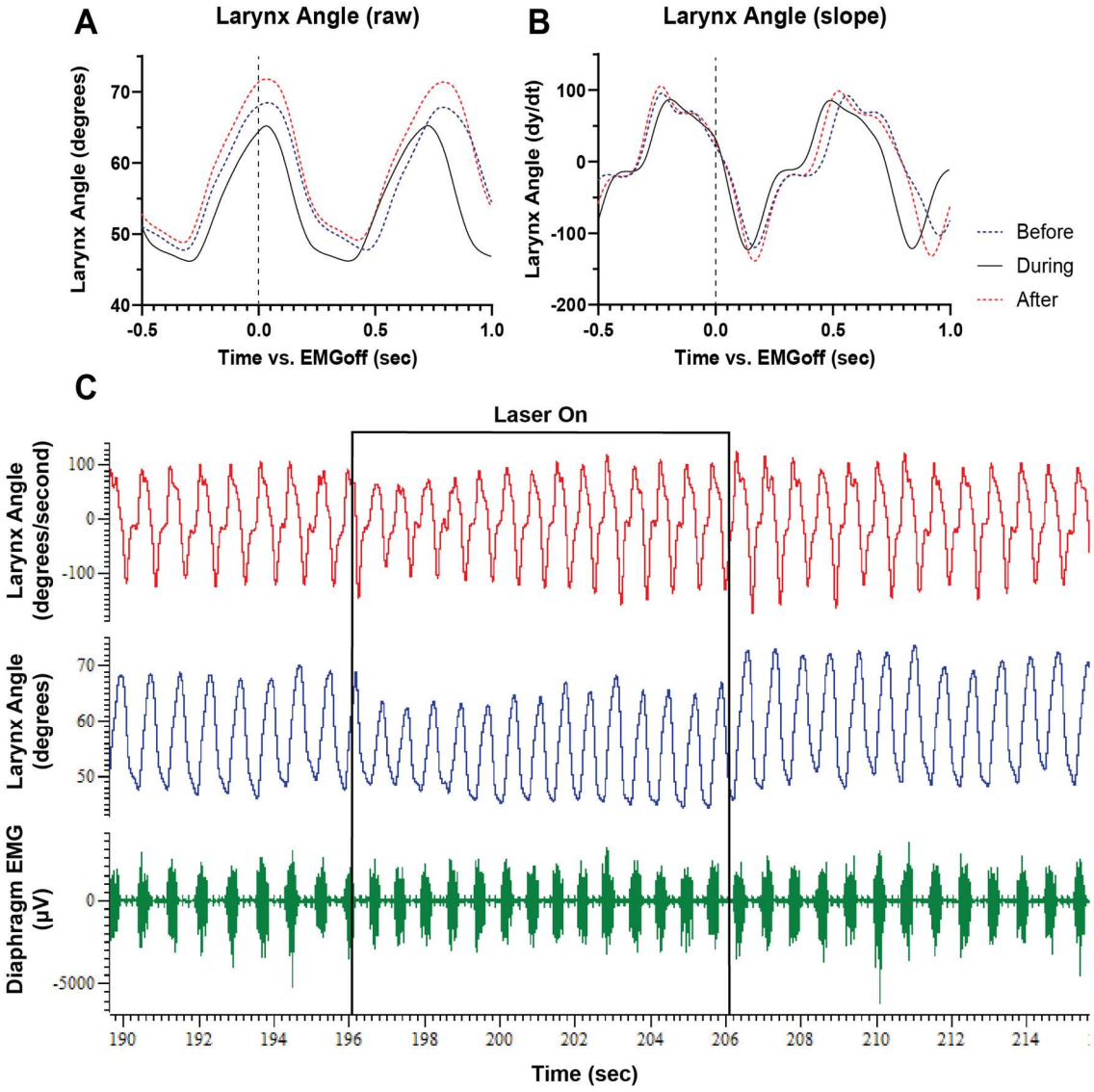

Figure 3.12: Raw (blue) and differentiated (red) traces of larynx angle and diaphragm EMG activity (green) before, during, and after 10 seconds of optogenetic IRt inhibition

Time of peak laryngeal adduction was measured from waveform averages above (Figure 3.12 B). During inhibition, post-I adduction occurred 30 ms earlier, and returned to baseline after inhibition.

3.3.3 Post-I vagal & sympathetic nerve activities during IRt inhibition

Electrophysiology recordings before, during, and after inhibition are shown in Figure 3.13 below. Phrenic-triggered waveform averages were created for vagus, sympathetic, and phrenic nerves 1 minute before, 1 minute during, and 1 minute after IRt inhibition (Figure 3.14). A clear absence of vagus post-I activity during inhibition was found. Sympathetic post-I activity was still present, though reduced in amplitude and occurring much earlier in the respiratory

cycle. Phrenic nerve activity showed a small decrease in amplitude, and an increase in duration of inspiratory burst. These effects were accompanied by a reduction in blood pressure.

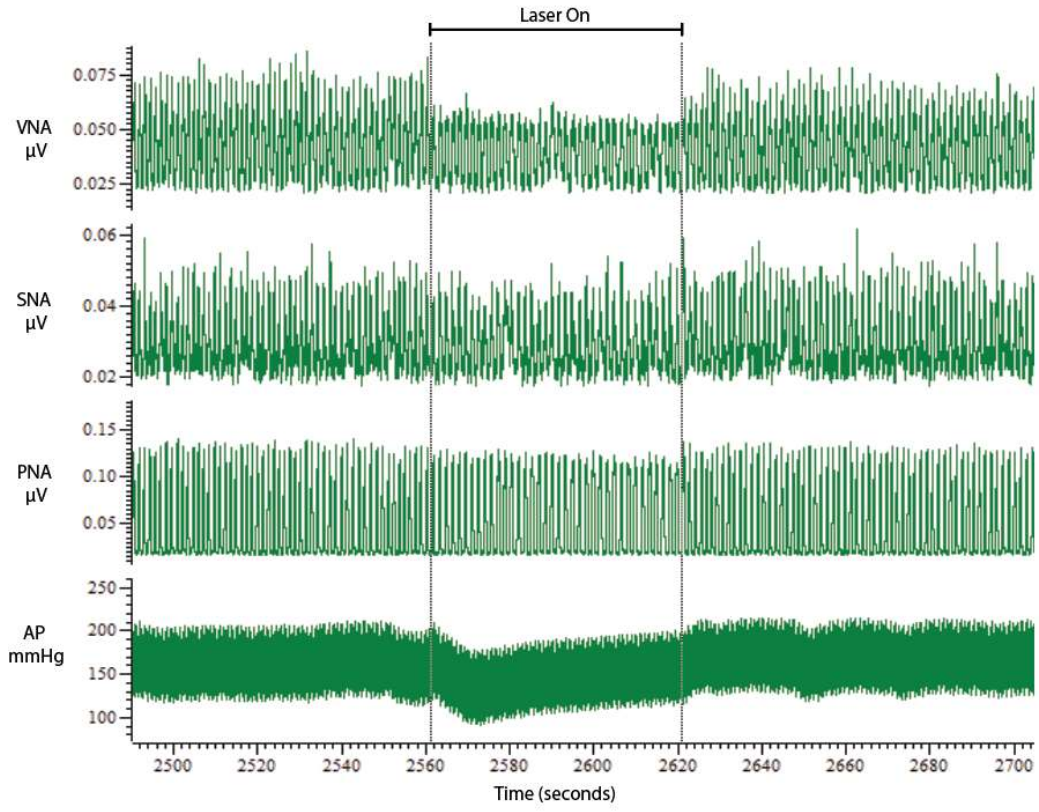

Figure 3.13: Vagus, sympathetic, and phrenic nerve recordings, and arterial blood pressure before, during, and after 1min optogenetic IRt inhibition. VNA=vagus nerve activity, SNA=sympathetic nerve activity (splanchnic), PNA=phrenic nerve activity AP= arterial blood pressure

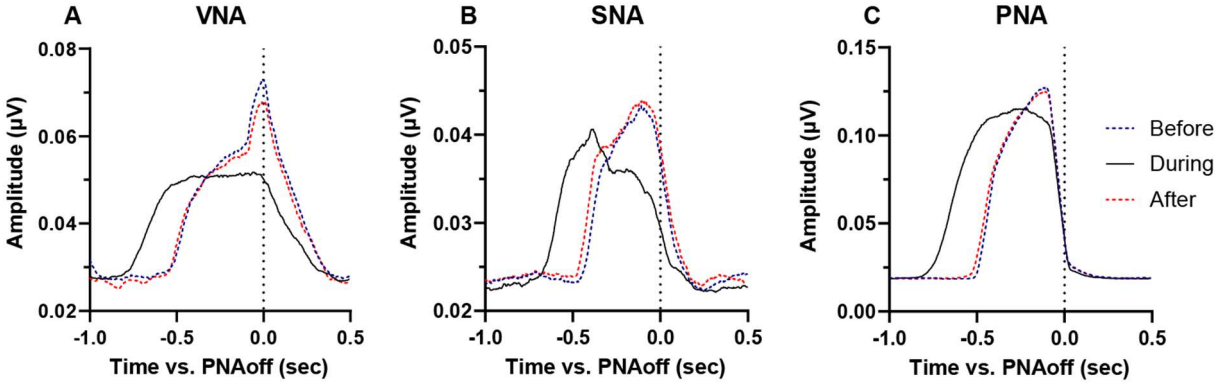

Figure 3.14: Phrenic-triggered waveform averages for vagus (A), sympathetic (B) and phrenic (C) nerve activity before, during, and after optogenetic IRt inhibition. VNA=vagus nerve activity SNA=sympathetic nerve activity PNA=phrenic nerve activity

Trough-to-peak vagus post-I amplitude was measured for 4 separate instances of inhibition, and compared before, during, and after the inhibition period.. One-way repeated measures ANOVA also found a significant effect for inhibition ($F(2,6)=33.17$, $p=0.0006$, $r2=0.92$). Multiple comparisons found that post-I VNA was significantly lower during IRt

inhibition compared to the 1 minute period immediately before (p=0.0021) and immediately after (p=0.0008) inhibition. There was no significant difference between post-I amplitude before and after inhibition (p=0.64).

3.3.4 Post-I timing

IRt inhibition appears to cause earlier sympathetic post-I peak activity (see Figure 3.14). One-way repeated measures ANOVA with multiple comparisons found a significant effect for inhibition in time of peak sympathetic ($F(2,6)=6.29$, $r^2=0.68$, $p=0.03$) activity, although multiple comparisons of sympathetic post-I time before, during, and after inhibition were not significant (Figure 3.15 B). This apparent shift in respiratory-sympathetic coupling could also be due to an increase in TI which has affected the graphs.

Vagus post-I time was also assessed using one-way repeated measures ANOVA with multiple comparisons (Figure 3.15 A). Vagus post-I time was significantly earlier during inhibition than before (p=0.037) and after (p=0.029), and one-way repeated measures ANOVA with multiple comparisons found a significant effect for inhibition ($F(2,6)=13.30$, $p=0.006$, $r^2=0.82$). However, time of peak vagal activity was difficult to measure during inhibition, as post-I spike was greatly reduced in amplitude.

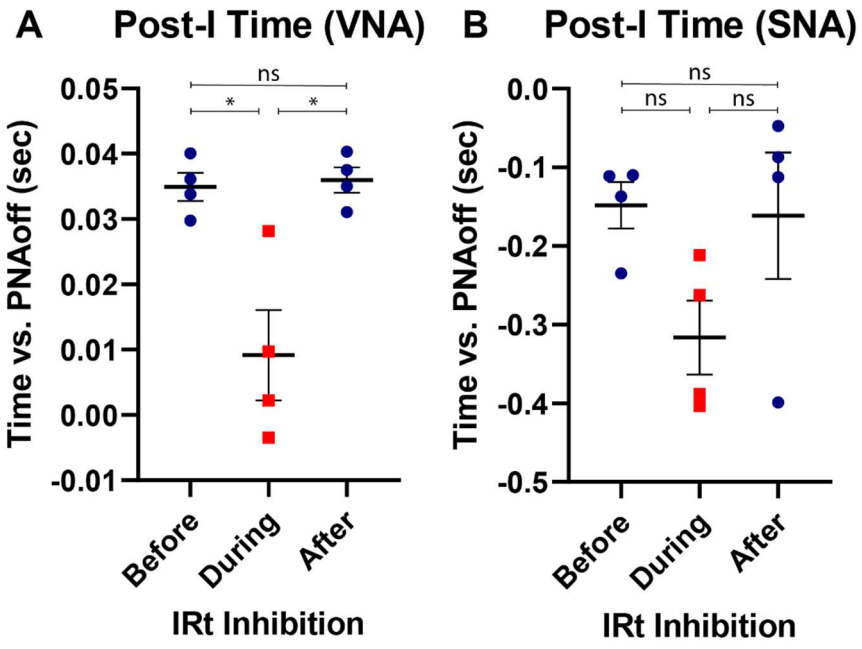

*Figure 3.15: Post-I vagus (A) and sympathetic (B) time before, during, and after 1 min optogenetic IRt inhibition. VNA=vagus nerve activity, SNA=sympathetic nerve activity, PNA=phrenic nerve activity, *=p<0.05, ns=p>0.05 error bars=SEM*

During hypoxemia trials, IRt inhibition resulted in delayed vagus post-I activity compared to hypoxemia alone (Figure 3.16 A). This contrasts with IRt inhibition alone (see Figure 3.16 A), which resulted in earlier vagus post-I. Sympathetic post-I time way delayed during hypoxemia but occurred earlier with hypoxemia and IRt inhibition (Figure 3.16 B).

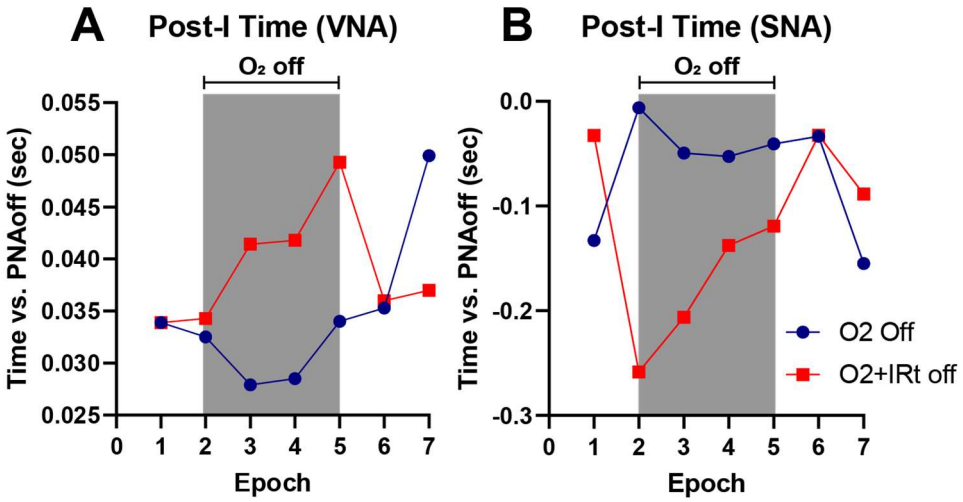

Figure 3.16 Post-I vagus (A) and sympathetic (B) time before, during, and after 1 min hypoxemia with and without optogenetic IRt inhibition. VNA=vagus nerve activity, SNA=sympathetic nerve activity, PNA=phrenic nerve activity

3.3.5 Respiratory Phase Timing

TI, TE, and Ttot were measured from phrenic nerve activity before, during, and after 1 minute of optogenetic IRt inhibition. As shown in Figure 3.17, TI and Ttot both increased during inhibition, before returning to near baseline levels.

Repeated measures one-way ANOVA found a significant effect for inhibition in TI ($F(2,6)=14.41$, $p=0.005$, $r^2=0.83$). Multiple comparisons found that during inhibition, TI was significantly longer than before ($p=0.007$) or after ($p=0.02$) inhibition. There was no significant difference in TI before and after inhibition ($p=0.7$) (Figure 3.17 A).

These changes in TI were also reflected in Ttot (Figure 3.17 C). One-way repeated measuresANOVA of showed a significant effect for inhibition ($F(2,6)=10.48$, $p=0.01$, $r^2=0.78$). Multiple comparisons found Ttot longer during inhibition than before ($p=0.02$) or after ($p=0.03$), with no difference between before and after ($p=0.9$).

No change in TE was seen in response to IRt inhibition, as shown in Figure 3.17 B. ANOVA found no significant effects or comparisons.

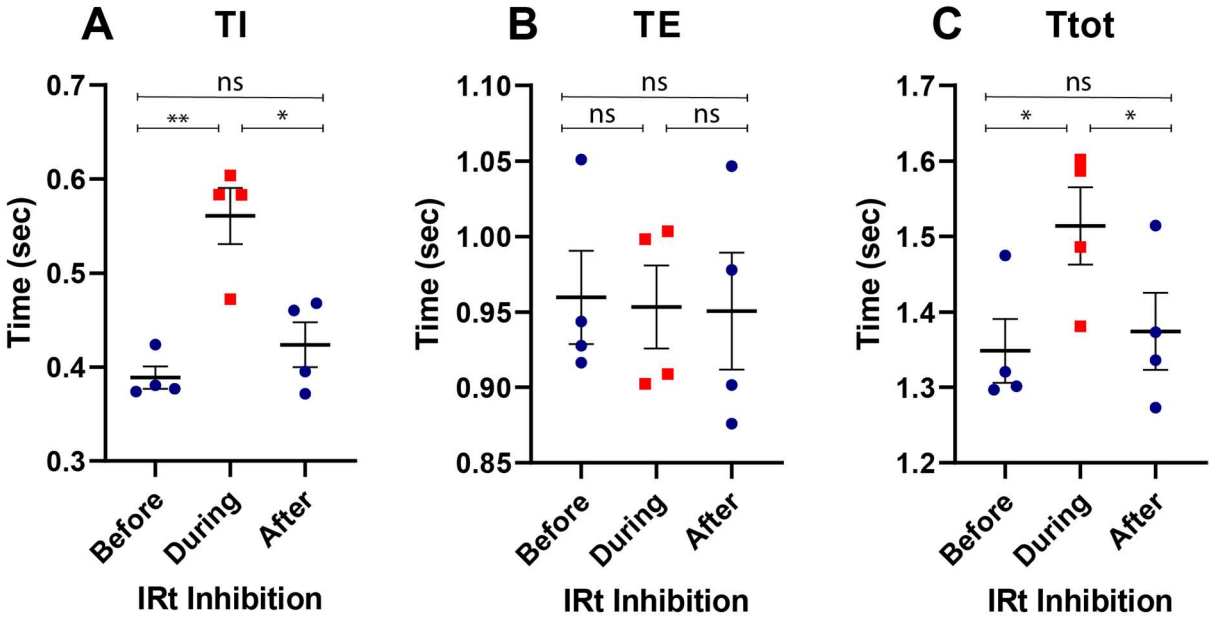

*Figure 3.17: Inspiration time (TI, A), expiration time (TE, B) and total respiratory cycle length (Ttot, C) for SHR responder before, during, and after optogenetic IRt inhibition, with mean and SEM. *=p<0.05, **=p<0.01*

IRt inhibition during hypoxemia caused an initial increase in TI and Ttot, but did not prevent the gradual decrease in TI, TE, or Ttot that occurred during hypoxemia alone (see Figure 3.18)

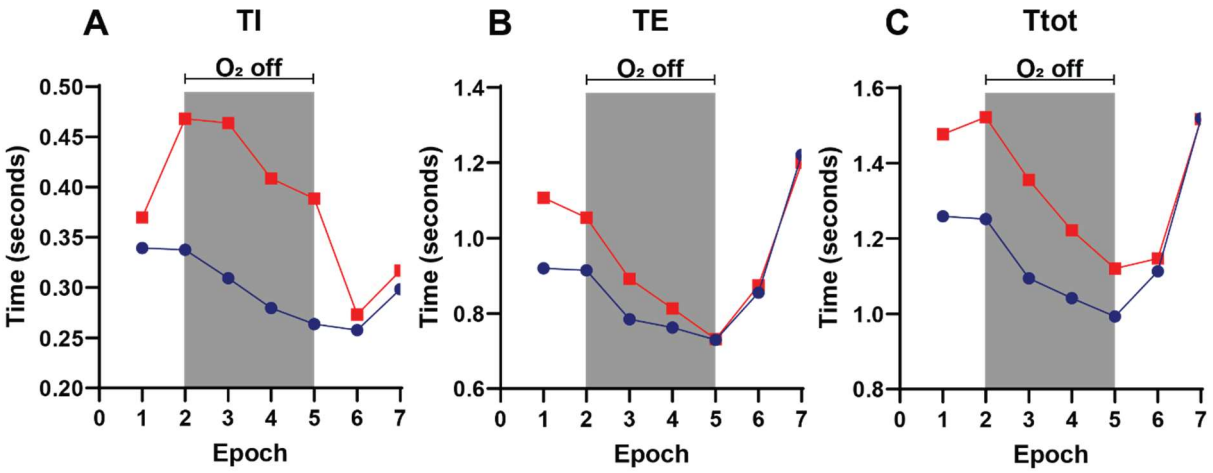

Figure 3.18: Inspiration time (TI, A), expiration time (TE, B) and total respiratory cycle length (Ttot, C) for SHR responder before, during, and after hypoxemia, with or without optogenetic IRt inhibition.

3.3.6 Blood Pressure

Optogenetic IRt inhibition resulted in decreased arterial blood pressure (Figure 3.19). One-way repeated measures ANOVAs were performed with multiple comparisons to determine

if this change was significant. Minimum and maximum arterial blood pressure were measured for 1 minute before, during, and after inhibition.

For systolic AP (Figure 3.19 A), ANOVA found a significant effect for inhibition ($F(2,6)=25.16$, $p=0.001$, $r^2=0.89$). Multiple comparisons found systolic blood pressure did not change from before to during inhibition ($p=0.85$), but rose significantly from during to after inhibition ($p=0.002$), rebounding above baseline ($p=0.004$). It took several minutes for to return to baseline levels, averaging 194 seconds. In one instance, blood pressure remained elevated and did not return to baseline.

For diastolic AP (Figure 3.19 B), ANOVA also found a significant effect for inhibition ($F(2,6)=57.1$, $p=0.0001$, $r^2=0.95$). Multiple comparisons found diastolic AP significantly lower during inhibition than before ($p=0.0002$) or after ($p=0.0005$). There was no difference in diastolic blood pressure between before and after ($p=0.29$).

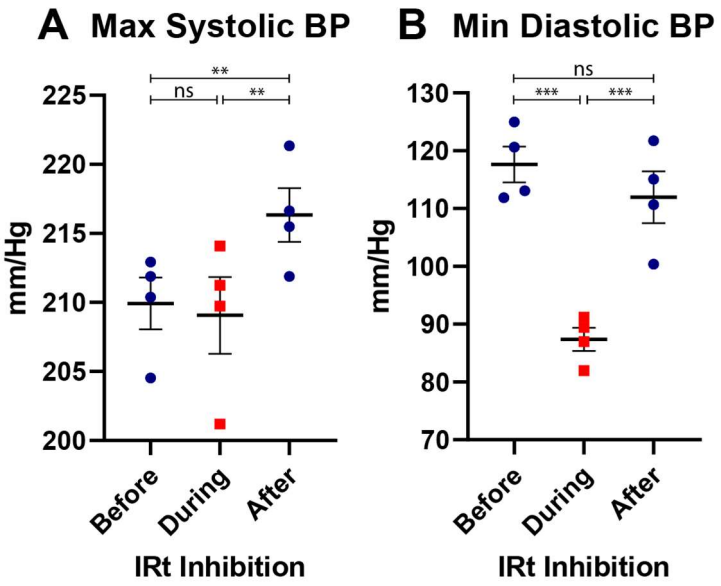

*Figure 3.19: Systolic (A) and diastolic (B) arterial blood pressure of SHR responder before, during, and after optogenetic IRt inhibition. **=p<0.01, ***=p<0.001, ns=p>0.05*

Optogenetic inhibition with hypoxemia resulting in an initial decrease in blood pressure (see Figure 3.20). Then, throughout the inhibition period, AP gradually rose in a similar pattern to that seen in hypoxemia alone.

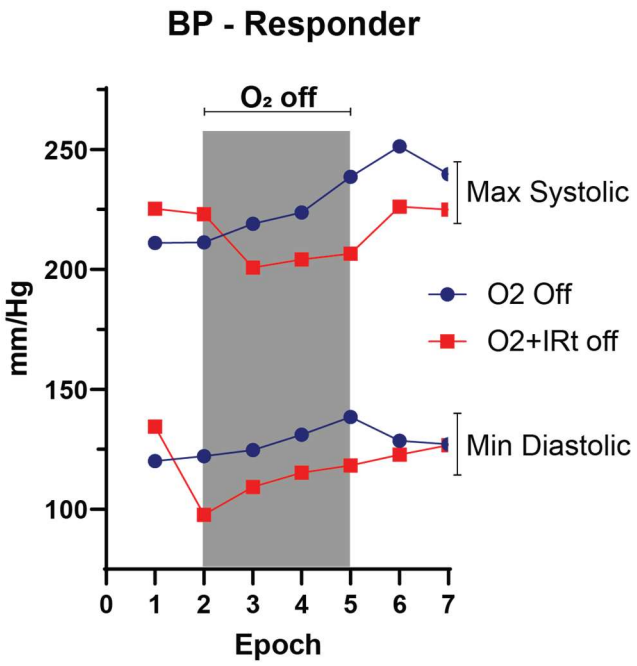

Figure 3.20: maximum systolic and minimum diastolic blood pressure throughout hypoxemia with and without IRt inhibition in SHR responder

4. Discussion:

4.1 Main findings

4.1.1 Overview

This project developed a non-invasive method of quantifying larynx activity for integration with simultaneously recorded diaphragm EMG. This was combined with vagus, sympathetic, and phrenic nerve recordings to investigate the role of post-I activity in driving post-I laryngeal adduction in the WKY and SHR rat, in order to determine whether the abnormal respiratory-sympathetic phenotype of the SHR could be attributed to shifting of the post-I phase of the respiratory cycle. In these experiments, SHRs and WKYs had similar patterns of laryngeal adduction, with no discernible difference identified.

During electrophysiology experiments, SHRs showed a temporal phase shift in respiratory-sympathetic coupling compared to WKYs, which was expected based on previous findings [6, 7, 42]. There was no difference in vagal post-I time between the two strains. This indicates that vagal post-I and respiratory-sympathetic coupling are two distinct mechanisms, despite usually occurring at the same time. This supports the hypothesis that temporal phase shift

in respiratory-sympathetic coupling seen in SHRs may reflect plastic changes in the innervation of sympathetic premotor neurons from excitatory inspiratory neurons.

Vagal post-I amplitude appeared higher in SHRs than WKYs, a finding that has not previously been reported. Optogenetic inhibition of the IRt reduced vagal post-I activity and arterial blood pressure in 1 SHR. IRt inhibition also caused a further temporal phase shift in respiratory-sympathetic coupling in the SHR, with peak activity occurring earlier within the respiratory cycle. This sheds further doubt on the theory that amplified KF or IRt activity is responsible for sympathetic dysregulation, as if this was the case IRt inhibition should have caused peak sympathetic activity to occur later, not earlier.

WKYs and SHRs also differed in their response to hypoxemia. SHRs had an increase in blood pressure, as demonstrated previously, while WKYs remained relatively stable. WKYs showed a temporal phase shift of vagal post-I activity during and after hypoxemia, which was not seen in SHRs. This indicates further dysfunction in SHR neural circuits, possible between chemoreceptive neurons in the RTN and neurons in the KF that drive post-I. This indicates that post-I activity may play a role in maintaining homeostasis, and the SHRs inability to alter post-I time may contribute to some of its numerous health problems.

Overall, these findings support Menuet and colleagues' [8] [13] theory that hypertension in SHRs is due to amplified excitatory connections between preBötC and the RVLM causing sympathetic activation during inspiration, rather than amplified post-I activity in the KF or IRt. It also demonstrates that vagal post-I activity and respiratory-sympathetic coupling may be generated by two separate mechanisms in the SHR.

4.1.2 Post-I laryngeal adduction persists in the absence of vagal post-I activity

It has been assumed that the post-inspiratory spike of activity seen in vagal motor neurons is analogous to post-I laryngeal adduction [9] [2]. However, the results of this study do not support this, as laryngeal adduction persisted (in the physiologically responsive rat during laryngeal recordings under isoflurane) despite IRt inhibition abolishing all vagal post-I activity

(in the same individual under urethane anaesthesia). It was expected that laryngeal adduction would cease during inhibition, which did not occur. While there was a small decrease in movement, perhaps reflecting a reduction in general tone of larynx, the gross pattern of laryngeal movement did not change. This indicates that vagal post-I activity is not necessarily representative of laryngeal activity.

4.1.3 Temporal phase shift of sympathetic activity in SHRs is exacerbated by IRt inhibition

This study found a temporal phase shift of respiratory-sympathetic coupling in SHRs, which was expected based on previous findings [6]. Sympathetic activity peaked during post-inspiration in WKYs but occurred during late inspiration in SHRs. Amplified respiratory-sympathetic coupling is thought to contribute to hypertension in the SHR [7]. Previous studies have found that inhibition of RVLM C1 neurons in SHRs reduces sympathetic amplitude, reverses the respiratory-sympathetic temporal phase shift, and reduces blood pressure to a normotensive range [42].

In these experiments, IRt inhibition in an SHR exacerbated temporal phase shift of respiratory-sympathetic coupling, with peak sympathetic activity occurring in early respiration at lower amplitude. This effect has not been seen in previous studies inhibiting this region in normotensive rats [11]. This suggests that respiratory-sympathetic coupling in the SHR is the result of a combination of post-I activity, as is the case in normotensive strains, combined with inspiratory-locked excitatory drive that is mechanistically independent of post-I activity.

4.1.4 SHRs have increased vagal post-I amplitude compared to WKYs, but no difference in post-I timing

Vagus nerve activity has not been directly compared between SHRs and WKYs before. In this study SHRs showed a higher amplitude of vagal post-I activity than WKYs. Optogenetic inhibition of the IRt abolished post-I activity completely, also resulting in decreased blood pressure. This suggests a potential link between the central mechanisms that underlie vagal post-I amplitude and blood pressure.

Due to temporal phase shift in sympathetic activity seen in SHRs, it was hypothesised that vagal post-I activity may also occur earlier in SHRs than WKYs. However, there was no difference in time of post-I activity (relative to phrenic nerve activity) between the two strains. This indicates that sympathetic dysregulation in SHRs is due to a mechanism that affects sympathetic activity only (potentially amplified excitatory connections between preBötC and the RVLM [13]), not due to overactivity in regions driving or transmitting post-I activity such as the KF or IRt.

4.1.5 Hypoxemia causes temporal phase shift of vagal post-I in WKYs but not SHRs, increases blood pressure in SHRs but not WKYs

In WKYs, hypoxemia caused a small temporal phase shift in vagal post-I activity. This was followed by a larger shift immediately after hypoxemia, with peak vagal activity during late expiration/early inspiration. Arterial blood pressure remained stable in WKYs throughout the hypoxemic protocol. In SHRs, there was no temporal shift in vagal post-I activity in response to hypoxemia, and arterial blood pressure increased.

It has been previously shown that hypoxemia increases the amplitude of vagal post-I activity and sympathetic activity in normotensive rats [11]. It has also been suggested that SHRs are in a constant hypoxic state, due to impaired blood delivery in brainstem areas such as the nucleus tractus solitarii [43]. This could explain why WKYs had a vagal response to hypoxemia while SHRs did not (as SHRs were already hypoxic). If SHRs are hypoxic under baseline conditions, oxygen-sensitive neurons (such as NTS neurons that receive input from peripheral chemoreceptors) may be already firing at maximum frequency and be unable to increase firing rate in response to hypoxemia. This is also supported by the higher vagal post-I amplitude seen in SHRs in this study.

4.1.6 IRt inhibition decreases respiratory frequency in SHRs, increases respiratory frequency in normotensive rats

IRt inhibition increased inspiration time in SHR, resulting in decreased respiratory frequency. Unfortunately, IRt inhibition was not successful in any WKYs, so it was not possible

to compare between the two strains. However, previous studies of IRt inhibition in the normotensive Lewis rat show slightly increased respiratory frequency due to a reduction in expiration time [11]. This apparent difference in effect could be due to a difference between SHRs and normotensive rats, or it could be due to off-target injections in this study. For example, in the current study some vector expression was seen in BötC, which drives expiration by inhibiting inspiratory activity. Inhibition of the BötC has previously been reported to delay the transition from inspiration to expiration, prolonging TI and reducing respiratory cycle frequency [44].

4.2 Limitations

4.2.1 Sample size

The biggest limitation in this study was small sample size, limiting the statistical power of analysis. Some biologically significant effects, such as increased vagal post-I amplitude in SHRs, were not found to be statistically significant due to low sample size. Due to this, care must be taken when interpreting these results. There is insufficient evidence to draw definitive conclusions from these experiments. However, these findings do provide insight into possible similarities and differences in respiratory/sympathetic coupling between SHRs and WKYs that are worth further investigation.

Surprisingly, in this study SHRs had lower sympathetic amplitude than WKYs. This contradicts previous findings that found increased sympathetic activity in SHR rats [7], and humans with hypertension [26] [5] [27]. This is likely an error, with only 3 WKYs an outlier may have influenced results. A larger sample size would have

4.2.2 Off-target injections

Originally, it was planned to compare the effects of optogenetic IRt inhibition between SHRs and WKYs. This was not possible as most animals were found to have off-target injections that missed the IRt. Interestingly, the only animal that had substantial IRt transduction was also the only animal in which a physiological response to IRt inhibition was visible. This animal was

an SHR, the effect of IRt inhibition on this individual was recorded and analysed, but could not be compared to WKY as a normotensive control.

Off-target injections appear too dorsal, with no ventral spread through the IRt. This could be due to tip of glass pipette breaking during facial mapping. This occurred several times during surgery, and injection depth was adjusted accordingly. It likely happened at other times and was not noticed. In future, this can be prevented by using a different electrode during facial mapping, and replacing pipette when ready for vector injection. Injection could also be performed in several small increments, moving up dorsally through the IRt instead of a single injection site.

The responder showed vector expression throughout the IRt, but also had significant spread into surrounding regions. Therefore, the effects of 'IRt inhibition' described in this study may be due to inhibition in other areas. Cells in the solitary tract showed reporter expression, but this is not a likely source of changes seen as optrodes were implanted deeper than the relatively dorsal solitary tract. Labelling was also seen in the nucleus ambiguus, solitary tract, and Bötzinger complex, and RVLM, which may have affected results.

4.2.3 Effect of anaesthesia

This study attempts to draw parallels between larynx activity recorded under isoflurane anaesthesia and nerve recordings performed under urethane anaesthesia. Urethane has minimal impact on respiration [45], while isoflurane has been shown to cause respiratory depression in rats [46], and is associated with laryngospasm in humans [47]. Placing a tube in the throat may have also affected laryngeal adduction. Due to this, larynx activity recorded in videos may not accurately reflect activity at the time of nerve recordings, or activity during conscious eupnoea.

Intraperitoneal urethane has also been shown to increase sympathetic output [48], lower systolic blood pressure [49], and reduce response to vagal stimulation [49]. Isoflurane also reduces blood pressure [50], but reduces sympathetic output [51]. To more accurately assess whether post-I laryngeal adduction continues in the absence of vagal post-I activity, laryngeal adduction and vagal nerve activity need to be recorded under the same type of anaesthesia. It is

not possible to perform larynx videos and nerve recording at the same time, due to the position of the animal. However, future experiments could record larynx activity under urethane before performing nerve recordings.

Some larynx videos were performed using a combination of ketamine and medetomidine for anaesthetic, however several animals overdosed and had to be resuscitated. WKYs were particularly vulnerable, experiencing adverse effects at approximately half the effective dose for SHRs. Due to the high risk of mortality, the used of ketamine/medetomidine was discontinued.

4.2.4 Recording of vagus nerve

The recurrent laryngeal nerve (RLN) branches from the vagus nerve to innervate the larynx [2]. Research on post-inspiratory activity tends to use the vagus nerve and RLN interchangeably, though vagus activity is not analogous to laryngeal adduction. As this project aimed to investigate the role of post-I activity in driving laryngeal adduction, recording from the RLN directly would have been more appropriate. However, the RLN is small, delicate, and difficult to isolate. The vagus nerve is easier to access surgically, and has previously been used as a substitute for RLN activity [11]. Recordings were performed distally to the RLN branch of the vagus nerve. It is possible that some post-I activity occurred in the RLN driving laryngeal adduction that was not present in the section of the vagus being recorded. Previous studies on IRt inhibition have only investigated vagus activity [11], not RLN.

4.3 Future Directions

4.3.1 Repeat experiment

These experiments should be repeated with more rats. As all of the non-responders had vector expression too dorsal, this indicates a systematic flaw in injection method, despite successful pilot experiments in which fluorescent beads were successfully deposited in the IRt. Target coordinates for facial nucleus mapping need to be refined, to increase proportion of on-target injections. Collecting data from more animals will increase the power of statistical analyses, and allow for comparison between WKYs and SHRs.

4.3.2 IRt excitation

Once the IRt has been successfully inhibited in multiple SHR and WKY rats, the next step is to examine the effect of IRt excitation. Photo stimulation of the region in normotensive mice has shown an increase in vagal activity, with a spike in activity occurring at the time of stimulation, regardless of respiratory phase [10]. This paper did not show the effect of IRt excitation of sympathetic activity or blood pressure.

4.3.3 Larynx activity with VNA, SNA, PNA

In these experiments, larynx videos with diaphragm EMG were performed first, followed by terminal electrophysiology. In future, I would like to record laryngeal adduction and nerve activity at the same time so they can be directly compared. This was not possible using the current method, as video requires animal suspended vertically while nerve recordings are performed with animal in prone position.

Pilot experiments were conducted using an inexpensive video endoscope, which could potentially be integrated with electrophysiology. This camera was low quality, and not able to clearly focus on the larynx. A very small medical grade endoscope would provide high quality larynx videos, but this is an expensive piece of equipment not available at the time these experiments were performed.

4.3.4 Clinical Applications

This project developed a method of quantifying larynx activity from video recordings using machine learning. This technique could be used to investigate a range of respiratory conditions that involve altered laryngeal adduction, such as sleep apnoea and chronic obstructive pulmonary disease. This could be utilised in a clinical setting to analyse videos obtained from patients during laryngeal endoscopy. It could also be adapted to examine activity in other upper airway muscles such as the tongue, or non-respiratory functions such as gastrointestinal peristalsis.

Additionally, these findings could contribute to identifying potential therapeutic targets for hypertension. My results suggest that pathways between inspiratory areas (PreBötC) and

sympathetic premotor neurons (RVLM) are a likely source of sympathetic dysregulation, not pathways driving post-I activity (KF, IRt). However, due to limited sample-size and off-target injections, further research must be conducted before clinical applications can be determined.

References

1. Dick, T.E., et al., *Cardiorespiratory Coupling*. 2014, Elsevier. p. 191-205.
2. Bautista, T.G., et al., *The Generation of Post-Inspiratory Activity in Laryngeal Motoneurons: A Review*. 2010, Springer New York. p. 143-149.
3. Anderson, E.A., et al., *Elevated sympathetic nerve activity in borderline hypertensive humans. Evidence from direct intraneural recordings.* Hypertension, 1989. **14**(2): p. 177-183.
4. Esler, M., G. Lambert, and G. Jennings, *Increased regional sympathetic nervous activity in human hypertension: causes and consequences.* J Hypertens Suppl, 1990. **8**(7): p. S53-7.
5. Esler, M., *The sympathetic system and hypertension*1.* American Journal of Hypertension, 2000. **13**(6): p. S99-S105.
6. Czyzyk-Krzeska, M.F. and A. Trzebski, *Respiratory-related discharge pattern of sympathetic nerve activity in the spontaneously hypertensive rat.* The Journal of Physiology, 1990. **426**(1): p. 355-368.
7. Simms, A.E., et al., *Amplified respiratory-sympathetic coupling in the spontaneously hypertensive rat: does it contribute to hypertension?* The Journal of Physiology, 2009. **587**(3): p. 597-610.
8. Menuet, C., et al., *Excessive Respiratory Modulation of Blood Pressure Triggers Hypertension.* Cell Metab, 2017. **25**(3): p. 739-748.
9. Ono, K., et al., *Synaptic origin of the respiratory-modulated activity of laryngeal motoneurons.* Neuroscience, 2006. **140**(3): p. 1079-1088.
10. Anderson, T.M., et al., *A novel excitatory network for the control of breathing.* Nature, 2016. **536**(7614): p. 76-80.
11. Toor, R.U.A.S., et al., *Neurons in the Intermediate Reticular Nucleus Coordinate Postinspiratory Activity, Swallowing, and Respiratory-Sympathetic Coupling in the Rat.* The Journal of Neuroscience, 2019. **39**(49): p. 9757-9766.
12. Smith, J.C., et al., *Spatial and Functional Architecture of the Mammalian Brain Stem Respiratory Network: A Hierarchy of Three Oscillatory Mechanisms.* Journal of Neurophysiology, 2007. **98**(6): p. 3370-3387.
13. Menuet, C., et al., *PreBötzinger complex neurons drive respiratory modulation of blood pressure and heart rate.* eLife, 2020. **9**.
14. Feldman, J.L., C.A. Del Negro, and P.A. Gray, *Understanding the Rhythm of Breathing: So Near, Yet So Far.* Annual Review of Physiology, 2013. **75**(1): p. 423-452.
15. Feldman, J.L. and C.A. Del Negro, *Looking for inspiration: new perspectives on respiratory rhythm.* Nature Reviews Neuroscience, 2006. **7**(3): p. 232-241.
16. Fogarty, M.J., C.B. Mantilla, and G.C. Sieck, *Breathing: Motor Control of Diaphragm Muscle.* Physiology, 2018. **33**(2): p. 113-126.
17. Kenny, B.J. and B. Bordoni, *Neuroanatomy, Cranial Nerve 10 (Vagus Nerve)*, in *StatPearls*. 2021, StatPearls Publishing

18. Dulak, D. and I.A. Naqvi, *Neuroanatomy, Cranial Nerve 7 (Facial)*, in *StatPearls*. 2021, StatPearls Publishing

19. Kim, S.Y. and I.A. Naqvi, *Neuroanatomy, Cranial Nerve 12 (Hypoglossal)*, in *StatPearls*. 2021, StatPearls Publishing

20. Smith, J.C., et al., *Brainstem respiratory networks: building blocks and microcircuits.* Trends in Neurosciences, 2013. **36**(3): p. 152-162.

21. Koizumi, H., et al., *Structural-Functional Properties of Identified Excitatory and Inhibitory Interneurons within Pre-Botzinger Complex Respiratory Microcircuits.* Journal of Neuroscience, 2013. **33**(7): p. 2994-3009.

22. Del Negro, C.A., G.D. Funk, and J.L. Feldman, *Breathing matters.* Nature Reviews Neuroscience, 2018. **19**(6): p. 351-367.

23. Dutschmann, M. and H. Herbert, *The Kölliker-Fuse nucleus gates the postinspiratory phase of the respiratory cycle to control inspiratory off-switch and upper airway resistance in rat.* European Journal of Neuroscience, 2006. **24**(4): p. 1071-1084.

24. Alshak, M.N. and M.D. J, *Neuroanatomy, Sympathetic Nervous System*, in *StatPearls*. 2021, StatPearls Publishing

25. Wachter, S.B. and E.M. Gilbert, *Beta-Adrenergic Receptors, from Their Discovery and Characterization through Their Manipulation to Beneficial Clinical Application.* Cardiology, 2012. **122**(2): p. 104-112.

26. Julius, S., et al., *Hyperkinetic borderline hypertension in Tecumseh, Michigan.* Journal of Hypertension, 1991. **9**(1): p. 77-84.

27. Kaye, D.M., et al., *Adverse consequences of high sympathetic nervous activity in the failing human heart.* Journal of the American College of Cardiology, 1995. **26**(5): p. 1257-1263.

28. Grassi, G., et al., *Dissociation Between Muscle and Skin Sympathetic Nerve Activity in Essential Hypertension, Obesity, and Congestive Heart Failure.* Hypertension, 1998. **31**(1): p. 64-67.

29. Wiesel, P., et al., *Two-kidney, one clip and one-kidney, one clip hypertension in mice.* Hypertension, 1997. **29**(4): p. 1025-30.

30. Zeng, J., et al., *Two-Kidney, Two Clip Renovascular Hypertensive Rats Can Be Used as Stroke-prone Rats.* Stroke, 1998. **29**(8): p. 1708-1714.

31. Henry, J.P., et al., *Psychosocial stress can induce chronic hypertension in normotensive strains of rats.* Hypertension, 1993. **21**(5): p. 714-723.

32. Dahl, L.K., M. Heine, and L. Tassinari, *Role of Genetic Factors in Susceptibility to Experimental Hypertension due to Chronic Excess Salt Ingestion.* Nature, 1962. **194**(4827): p. 480-482.

33. Nishijima, Y., et al., *Characterization of blood pressure and endothelial function in TRPV4-deficient mice with l -NAME- and angiotensin II-induced hypertension.* Physiological Reports, 2014. **2**(1): p. e00199.

34. Mullins, J.J., J. Peters, and D. Ganten, *Fulminant hypertension in transgenic rats harbouring the mouse Ren-2 gene.* Nature, 1990. **344**(6266): p. 541-544.

35. Leong, X.F., C.Y. Ng, and K. Jaarin, *Animal Models in Cardiovascular Research: Hypertension and Atherosclerosis.* Biomed Res Int, 2015. **2015**: p. 528757.

36. Okamoto, K. and K. Aoki, *Development of a Strain of Spontaneously Hypertensive Rats.* Japanese Circulation Journal, 1963. **27**(3): p. 282-293.

37. Trippodo, N.C. and E.D. Frohlich, *Similarities of genetic (spontaneous) hypertension. Man and rat.* Circulation Research, 1981. **48**(3): p. 309-319.

38. Watakabe, A., et al., *Comparative analyses of adeno-associated viral vector serotypes 1, 2, 5, 8 and 9 in marmoset, mouse and macaque cerebral cortex.* Neuroscience Research, 2015. **93**: p. 144-157.

39. Turner, A., et al., *Rostroventrolateral medulla neurons with commissural projections provide input to sympathetic premotor neurons: anatomical and functional evidence.* European Journal of Neuroscience, 2013. **38**(4): p. 2504-2515.

40. Brown, D.L. and P.G. Guyenet, *Electrophysiological study of cardiovascular neurons in the rostral ventrolateral medulla in rats.* Circ Res, 1985. **56**(3): p. 359-69.

41. Mathis, A., et al., *DeepLabCut: markerless pose estimation of user-defined body parts with deep learning.* Nature Neuroscience, 2018. **21**(9): p. 1281-1289.

42. Menuet, C., et al., *Excessive Respiratory Modulation of Blood Pressure Triggers Hypertension.* Cell Metabolism, 2017. **25**(3): p. 739-748.

43. Hosford, P.S., et al., *Abnormal oxygen homeostasis in the nucleus tractus solitarii of the spontaneously hypertensive rat.* Experimental Physiology, 2017. **102**(4): p. 389-396.

44. Burke, P.G.R., et al., *Somatostatin selectively ablates post-inspiratory activity after injection into the Bötzinger complex.* Neuroscience, 2010. **167**(2): p. 528-539.

45. Maggi, C.A. and A. Meli, *Suitability of urethane anesthesia for physiopharmacological investigations. Part 3: Other systems and conclusions.* Experientia, 1986. **42**(5): p. 531-537.

46. Imai, A., et al., *Assessment of isoflurane-induced anesthesia in ferrets and rats.* American journal of veterinary research, 1999. **60**(12): p. 1577-1583.

47. Al-alami, A.A., M.M. Zestos, and A.S. Baraka, *Pediatric laryngospasm: prevention and treatment.* Current Opinion in Anesthesiology, 2009. **22**(3): p. 388-395.

48. Maggi, C.A. and A. Meli, *Suitability of urethane anesthesia for physiopharmacological investigations in various systems Part 1: General considerations.* Experientia, 1986. **42**(2): p. 109-114.

49. Maggi, C.A. and A. Meli, *Suitability of urethane anesthesia for physiopharmacological investigations in various systems. Part 2: Cardiovascular system.* Experientia, 1986. **42**(3): p. 292-297.

50. Poon, Y.-Y., et al., *Disproportional cardiovascular depressive effects of isoflurane: Serendipitous findings from a comprehensive re-visit in mice.* Lab Animal, 2021. **50**(1): p. 26-31.

51. J, et al., *Sympathetic Efferent Nerve Activity in Conscious and Isoflurane-anesthetized Dogs.* Anesthesiology, 1984. **61**(3): p. 266-270.